4. F-5 CFD RESULTS

Michael J de C Henshaw
British Aerospace (Operations) Ltd.
Military Aircraft and Aerostructures,
Brough, East Riding of Yorkshire,
HU15 1EQ
UK
michael.henshaw@bae.co.uk

Stephane Guillemot
Dassault Aviation
78, Quai Marcel Dassault,
F-92214, Saint Cloud,
CEDEX
France
stephane.guillemot@dassault-aviation.fr

NOMENCLATURE

α	Angle of attack (deg.)	C_r	Root chord (=0.6396 m)
κ	Reduced frequency ($=\pi FC_r/V_\infty$)	F	Frequency of modal oscillation (Hz)
θ	Maximum pitch angle (deg.)	M	Mach number
η	Normalised spanwise co-ordinate (=y/s)	Re	Reynold's number based on the mean geometric chord.
$\overline{C}$	Mean geometric chord (=0.4183m)		
C_l	Lift coefficient	s	Span of wing
Cp	Pressure coefficient	V_∞	Free-stream velocity (m/s)
CpImag	Imaginary part of pressure coefficient for unsteady pressures	y	Spanwise co-ordinate
		Y+	Normalised wall distance of first cell height
CpReal	Real part of pressure coefficient for unsteady pressures		

See definitions in chapter 5.

INTRODUCTION

The F-5 test series (see chapter 5) provides a succession of geometries of increasing complexity [Ref. 1, Ref. 2], which will be useful for validating CFD codes during their development. In this chapter a range of CFD results are provided for the clean wing configuration at selected flow conditions, and a more limited set for one complex configuration. Results from essentially state of the art UTSP (Unsteady Transonic Small Perturbation), Full Potential, Euler, and NS (Navier-Stokes) codes are presented, this will allow the reader to gauge anticipated modelling accuracy for code development purposes. Table 1 summarises the methods used by contributors reported herein, the methods themselves are described in a standard pro-forma and the results collated as a series of plots. The flow conditions calculated are summarised in Table 2 and Table 4. Two or more methods are presented for each level of modelling approximation in order to assist the reader in gauging the likely level of variation in solution at a particular level of approximation.

Level of approximation	Contributor organisation	Method name/ identification label	Method type
UTSP	BAe.	UTSPV21	Cartesian/finite difference
UTSP	NASA	CAP-ASP	Cartesian/finite difference
Full Potential	CIRA	HELIFP	Structured/finite volume
Full Potential	Dassault Aviation	TCITRON	Structured/finite difference
Euler	INTA	EUL3DU	Structured/explicit/multiblock
Euler	Glasgow University	PMB3D	Structured multiblock/implicit
Euler	Dassault Aviation	EUGENIE	Unstructured finite volume / implicit
Euler	BAe.	UEMB	Structured/explicit/multiblock
Euler	NASA	ENS3DAE	Structured/finite difference
Navier-Stokes	NASA	ENS3DAE	Structured/finite difference

Table 1 CFD Methods

CFD METHODS

DESCRIPTIONS OF CODES

A table of information is provided for each CFD code, which will allow the reader to make comparisons with codes under development. The first section of the code formulary gives a general description of the method type, but in the case of the NS code, only the turbulence and transition modelling actually used for data presented herein are described (additional models may also be available). The manner in which convergence is determined is described in item 1.10, and techniques used to accelerate the overall convergence of the method are also specified (item 1.6). Where available, performance data is also provided (items 4.2-4.4), and coupled with information of platform (item 4.1) the reader will be able to gauge, in a general manner, the comparative performance of newly developing computing techniques with the contemporary techniques reported herein.

Section 2 of the code formulary gives details about the specific grid used in the studies reported here; where the grid is completely structured the grid dimensions are given as chordwise X spanwise X normal. The grid size is specified as number of cells, number of vertices, or both. Any modifications to the geometry (e.g. treatment of wing tip) are noted in item 2.6.

The presentation of the results is detailed below; only a limited number of CFD solutions have been plotted in this written report, but many more are plotted in the electronic report. In section 3 of the code formulary the run numbers (as indexed in chapter 5) of those cases presented in either the written or electronic report are listed.

Interpolation details are provided where interpolation from CFD grid locations to specific points has taken place (item 3.3). Where no interpolation has been used, the data is extracted directly from the computational grid points (vertices or cell centres as appropriate to that particular method).

UTSP CODES

1 CODE

	UTSPV21
1.1 Type	UTSP (Unsteady Transonic Small Perturbation)
1.2 Name	UTSP v2.1
1.3 Description	Inviscid, linearised or non-linear TSP equations for single lifting surface with up to 2 control surfaces.
1.4 Available grid types	Geometry transformed to rectangular wing with 60 X 20 X 40 grid dimensions for optimised performance.
1.5 Artificial viscosity	None
1.6 Convergence acceleration techniques	None
1.7 Turbulence model	N/A
1.8 Transition model	N/A
1.9 Time-step	The Mach number and the planform geometry determine the allowable Δt for stability, with the leading edge sweep having a particularly strong influence. For the F-5 case a value of Δt=0.002 has been used.
1.10 Convergence	Not specified
1.11 References	Ref. 10

2 GRID

2.1 Size of grid	120 X 20 X 40
2.2 Y+	N/A
2.3 Number of Surface grid points	78 X 17 (i.e. 39 on each surface)
2.4 Grid type	C-grid (transformed)
2.5 Distance of outer boundaries from the wing	Not specified
2.6 Modifications to geometry	None

3 RESULTS

3.1 Written Report	152 (sections 1,3,5,7), 370 (1 & 7)
3.2 Electronic data	138 (sections 1-8), 152 (1-8), 191 (1-8), 370 (1 & 7)
3.3 Interpolation details	Linear interpolation to spanwise station

4 ADDITIONAL INFORMATION

4.1 Platform	Cray YMP
4.2 CPU	
4.2.1 Total	Not given
4.2.2 per iteration	Not given
4.2.3 per cycle	Not given
4.3 Convergence	Not given
4.4 Memory	Not given
4.5 Contact for further information	M J de C Henshaw, British Aerospace (Operations) Ltd, Military Aircraft and Aerostructures, Brough, East Riding of Yorkshire, HU15 1EQ, UK. michael.henshaw@bae.co.uk

1 CODE

CAP-ASP

1.1 Type	UTSP
1.2 Name	CAP-ASP
1.3 Description	Advanced TSP with revised streamwise flux and revised mass-flux boundary conditions. Boundary conditions applied on mean plane. AF algorithm for finite difference solution.
1.4 Available grid types	Single Cartesian grid mapped to plan-form
1.5 Artificial viscosity	None
1.6 Convergence acceleration techniques	N/A
1.7 Turbulence model	N/A
1.8 Transition model	N/A
1.9 Time-step	On the order of .01 or .02 (only steady cases provided)
1.10 Convergence	Residual reduced to E-4 to E-5 (3-4 orders of magnitude)
1.11 References	None - derivative of CAP-TSD. Ref. 6

2 GRID

2.1 Size of grid	180 X 45 X 90 = 729 000 grid points
2.2 Y+	N/A
2.3 Number of Surface grid points	90 X 30 = 2700 each on upper and lower surface
2.4 Grid type	Single Cartesian grid mapped to plan-form
2.5 Distance of outer boundaries from the wing	10 root chords upstream, downstream, above, and below the wing. 2 semi-spans
2.6 Modifications to geometry	None; airfoil constant throughout including tip

3 RESULTS

3.1 Written Report	137 (sections 1,3,5,7), 152 (1,3,5,7), 168 (1,3,5,7)
3.2 Electronic data	137, 138, 152, 158, 168, 190, 191 (steady runs only, sections 1 -

	8)
3.3 Interpolation details	Linear spanwise interpolation on unit square to measurement chords

4 ADDITIONAL INFORMATION

4.1 Platform	Cray C-90
4.2 CPU	
4.2.1 Total	2000-4000 time steps required on the order of 1500-3000 sec
4.2.2 per iteration	.75 sec
4.2.3 per cycle	N/A
4.3 Convergence	Varied by case, see 1.10
4.4 Memory	31 mega words
4.5 Contact for further information	R. Bennett, Aeroelasticity Branch, Structures Div., NASA, Mail stop 340, NASA Langley Research Center, Hampton, VA. 23681-2199 , USA r.m.bennett@larc.nasa.gov

FULL POTENTIAL CODES

1 CODE

HELIFP

1.1 Type	Unsteady Full Potential equation in conservative form.
1.2 Name	HELIFP Developed by CIRA, DERA, NLR, PML GKN-Westland, AGUSTA during the BRITE/EURAM project HELISHAPE(1993-96)
1.3 Description	Finite volume discretisation with velocity potential at the vertex and flux quantities at the cell centre.
1.4 Available grid types	Structured C-H topology.
1.5 Artificial viscosity	Streamwise density flux biasing.
1.6 Convergence acceleration techniques	Approximate factorisation with Newton iterations.
1.7 Turbulence model	N/A
1.8 Transition model	N/A
1.9 Time-step	CFL number 100-->500
1.10 Convergence	Two convergence criteria are used in HELIFP: the correction of the velocity potential between two pseudo-time steps, and the behaviour of the number of supersonic points in the field. For transonic cases the second method is more reliable.
1.11 References	Ref. 3, Ref. 4

2 GRID

2.1 Size of grid	161 X 32 X 24
2.2 Y+	N/A
2.3 Number of Surface grid points	116 X 22
2.4 Grid type	C-H
2.5 Distance of outer boundaries from the wing	Distance of C-outer boundary = 7 root chords Location of the last H-outer boundary = 1.5 semi-span
2.6 Modifications to geometry	Linear closing of T.E. sharp closing of wing tip.

3 RESULTS

3.1 Written Report	152 (sections 1,3,5,7 + convergence plots), 370 (1 & 7), 373 (1 & 7), 383 (1 & 7)
3.2 Electronic data	151, 152, 168, 190, 160, 172, 370, 373, 383 (sections 1 – 8)
3.3 Interpolation details	Pressure coefficients linearly interpolated onto experimental stations.

4 ADDITIONAL INFORMATION

4.1 Platform	SGI Power Challenge
4.2 CPU	
4.2.1 Total	(RUN 370): 8540 sec
4.2.2 per iteration	(RUN 370): 2.527 sec
4.2.3 per cycle	(RUN 370): 3638 sec.
4.3 Convergence	N. iterations (RUN 370): 3380 (500 convergence +2 cycles of 720 steps with 2 Newton it. = 500 + 2880)
4.4 Memory	85 Mb
4.5 Contact for further information	A Pagano, Aerodynamics and Propulsion department, CIRA, Via Maiorise, 81043, Capua, CE, Italy. a.pagano@cira.it

1 CODE

TCITRON

1.1 Type	Full Potential
1.2 Name	TCITRON
1.3 Description	Finite difference discretisation based on a non-conservative formulation with implicit time and semi-implicit space schemes. 3D, but only for wing geometries (with a wake surface). Steady Boundary Layer coupling capability. Resolution of the dynamic aeroelasticity equation in a reduced modal basis. Unsteady motion is applied through a transpiration boundary condition.
1.4 Available grid types	Structured C-H topology type.
1.5 Artificial viscosity	Due to non-conservative formulation
1.6 Convergence acceleration techniques	Full multigrid scheme (3 levels)
1.7 Turbulence model	N/A
1.8 Transition model	N/A
1.9 Time-step	From 12 to 360 Δt / cycles
1.10 Convergence	6 orders of perturbation potential correction
1.11 References	

2 GRID

2.1 Size of grid	185 X 21 X 22
2.2 Y+	N/A
2.3 Number of Surface grid points	113 X 14
2.4 Grid type	C-H
2.5 Distance of outer boundaries from the wing	Distance of C-outer boundary = from 5 to 8 root chords Location of the last H-outer boundary = 1.5 semi-span

2.6 Modifications to geometry	Tip fairing is modelled, but with closure 4mm from the experimental tip.

3 RESULTS

3.1 Written Report	137, 152, 168 (sections 1,3,5,7), 370 (1 & 7)
3.2 Electronic data	137, 138, 151, 152, 158, 168, 160, 370, 383 (sections 1 – 8)
3.3 Interpolation details	Spanwise grid distribution adjusted to coincide with experimental stations. No interpolation needed

4 ADDITIONAL INFORMATION

4.1 Platform	SGI O_2 (R 10000)
4.2 CPU	
4.2.1 Total	(RUN 370): 1570 sec (2 cycles)
4.2.2 per iteration	(RUN 370): 1.18 sec
4.2.3 per cycle	(RUN 370): 765 sec.
4.3 Convergence	300 steady iterations + 2 cycles of 72 x 10 unsteady iterations
4.4 Memory	12 Mb
4.5 Contact for further information	S. Guillemot, Dassault Aviation - 78, Quai Marcel Dassault, F-92214, Saint Cloud, CEDEX, France. Stephane.guillemot@dassault-aviation.fr

EULER CODES

Five Euler methods have been used, although not all are represented in the written report. There are four structured grid codes, of which three are multiblock, and one unstructured grid code. Two of the codes (ENS3DAE and PMB3D) are in fact Navier-Stokes codes, but for the purposes of this set of results they have been run in Euler mode. This sample of methods covers explicit, semi-implicit and fully implicit formulations.

1 CODE

EUL3DU

1.1 Type	Euler
1.2 Name	EUL3DU
1.3 Description	Finite-Volume, Cell centred, 2nd order central flux approximation, 2nd order 5 stage Runge-Kutta time integration. Unsteady motion is introduced through moving grid: grid is fixed at the outer boundary, but follows wing movement at inner boundary. Smooth transition in between outer and inner boundaries that ensures geometry conservation law is satisfied.
1.4 Available grid types	Structured O-H, monoblock.
1.5 Artificial viscosity	Jameson's type blending of 2nd and 4th order terms
1.6 Convergence acceleration techniques	Implicit residual smoothing, dual time-stepping, local time stepping (steady only), enthalpy damping (steady only).
1.7 Turbulence model	N/A
1.8 Transition model	N/A
1.9 Time-step	Maximum local Δt^* (dimensionless time with root chord and free-stream velocity) corresponding to a CFL of 6 for steady cases. Δt^*=0.001 for unsteady cases (dual time stepping not used), selected for accuracy, not for stability reasons.

1.10 Convergence	5000 Iterations with a reduction in maximum residual of at least 6 orders of magnitude for steady cases (Figure 4a). 3 periods for unsteady cases, the last period is Fourier analysed (Figure 4c)
1.11 References	Ref. 5

2 GRID

2.1 Size of grid	160 x 31 x 32 cells
2.2 Y+	N/A
2.3 Number of Surface grid points	160 x 21
2.4 Grid type	O-H
2.5 Distance of outer boundaries from the wing	9 root-chords / 2 semi-span
2.6 Modifications to geometry	Linear closing of T.E. Sharp closing of wing tip

3 RESULTS

3.1 Written Report	137, 168 (sections 1,3,5,7), 152 (1,3,5,7,8 + convergence plots), 172 (convergence plots), 370, 373, 383 (1 & 7)
3.2 Electronic data	137, 138, 151, 152, 158, 168, 190, 191, 383, 370, 160, 373, 172, 193 (sections 1-8)
3.3 Interpolation details	Spanwise grid distribution adjusted to coincide with experimental stations. No interpolation needed

4 ADDITIONAL INFORMATION

4.1 Platform	Cray YMP-EL
4.2 CPU	
4.2.1 Total	10900 secs. (Case 152, 5000 iterations)
4.2.2 per iteration	13.7×10^{-6} secs. /cell/iteration
4.2.3 per cycle	58890 secs. (Case 172, 27000 iterations)
4.3 Convergence	See 1.10 above.
4.4 Memory	8 MWords
4.5 Contact for further information	L P Ruiz-Calavera, INTA, Aerodynamics Division, Carretera de Ajalvir Km 4.5, 28850 Torrejon de Ardoz, SPAIN. ruizcl@inta.es

1 CODE

PMB3D

1.1 Type	Euler
1.2 Name	PMB3D
1.3 Description	A fully Implicit structured, cell-centred Parallel multiblock solver. The convective terms are discretised using Osher's upwind flux difference splitting scheme with MUSCL variable extrapolation. The unsteady equations solved using the classical dual time method introduced by Jameson Unsteady motion introduced by rigid rotation of the grid with the boundary velocities, using a first order difference.
1.4 Available grid types	Structured multiblock

1.5 Artificial viscosity	Through Van-Albada Limiting of MUSCL
1.6 Convergence acceleration techniques	The Implicit Jacobian matrix is approximated to reduce storage and is solved using a Krylov subspace method preconditioned with BILU(0). Only the pre-conditioned is decoupled across blocks
1.7 Turbulence model	N/A
1.8 Transition model	N/A
1.9 Time-step	Explicit start-up 0.4 Implicit 250. With at least 3 Cycles for unsteady runs.
1.10 Convergence	Steady cases are 8 orders in the L2 norm of the starting residual. Unsteady results are 6 orders. See Figure 4.
1.11 References	Ref. 12, also http://www.aero.gla.ac.uk/Research/CFD

2 GRID

2.1 Size of grid	180224 nodes, 225888 cells
2.2 Y+	N/A
2.3 Number of Surface grid points	84 X 34 = 2,856 cells
2.4 Grid type	Multiblock
2.5 Distance of outer boundaries from the wing	10 (root) chords streamwise and normal to wing, 3 spans from wing tip in spanwise direction.
2.6 Modifications to geometry	Tip fairing modelled, but with closure 4mm from experimental tip.

3 RESULTS

3.1 Written Report	152 (sections 1,3,5,7, + convergence plots), 172 (convergence plots), 370 (1 & 7)
3.2 Electronic data	138, 152, 191, 383, 370, 160, 373, 193 (sections 1 – 8)
3.3 Interpolation details	Linear interpolation in spanwise direction to measurement stations.

4 ADDITIONAL INFORMATION

4.1 Platform	Ppro 200's
4.2 CPU	5-7 work units per implicit iteration.
4.2.1 Total	Not given
4.2.2 per iteration	Not given
4.2.3 per cycle	Not given
4.3 Convergence	Explicit start up, followed by implicit to converge to at least 6 orders of magnitude on residuals. At least 3 cycles used for unsteady. See Figure 4.
4.4 Memory	2.1 Kbytes per cell
4.5 Contact for further information	B E Richards, Aerospace Engineering, James Watt Building, Glasgow University, Glasgow, Scotland, G12 8QQ, UK. bryan@aero.gla.ac.uk

1 CODE

EUGENIE

1.1 Type	Euler
1.2 Name	EUGENIE
1.3 Description	Galerkin finite volume approx. using a modified Lax-Wendroff scheme with implicit low storage time integration for steady,

	implicit 2nd order time integration (Gear method) for unsteady calculations.
	For steady flow calculations viscous effects are included using a boundary layer method: Laminar and Turbulent Boundary Layer with integral method. Boundary Layer coupling with "transpiration" velocities.
	Unsteady motion applied using a transpiration boundary condition.
1.4 Available grid types	Unstructured
1.5 Artificial viscosity	2nd order Lax-Wendroff
1.6 Convergence acceleration techniques	Jacobi method and dual time stepping strategy
1.7 Turbulence model	N/A
1.8 Transition model	Granville criteria for smooth transition and modified with Schlichting correction for roughness. Used for viscous coupled calculations.
1.9 Time-step	Corresponding to a maximum CFL of 10 / Δt.
1.10 Convergence	L_2 residual on all the variables (5 orders)
1.11 References	Paper to appear in M^2AN

2 GRID

2.1 Size of grid	51 539 nodes, 294 851 cells
2.2 Y+	N/A
2.3 Number of Surface grid points	2 865
2.4 Grid type	Unstructured
2.5 Distance of outer boundaries from the wing	Between 10 to 15 root chord.
2.6 Modifications to geometry	Tip fairing is modelled, but with closure 4mm from the experimental tip.

3 RESULTS

3.1 Written Report	Euler: 370, 373, 383 (sections 1 & 7),
	Euler+boundary layer: 137, 152, 168 (1,3,5,7)
3.2 Electronic data	137, 138, 151, 152, 158, 168, 190, 191
	383, 370, 160, 373, 172, 193. (1 - 8)
3.3 Interpolation details	Pressure coefficients interpolated onto experimental stations.

4 ADDITIONAL INFORMATION

4.1 Platform	IBM SP2
4.2 CPU	All CPU times given for 1 processor
4.2.1 Total	(RUN 370): 27,440 sec ≈ 7h30 (2 cycles)
4.2.2 per iteration	(RUN 370): 12.25 sec.
4.2.3 per cycle	(RUN 370): 8,200 sec ≈ 2h30
4.3 Convergence	4 orders on L_2 residual for unsteady steps.
4.4 Memory	65 Mb
4.5 Contact for further information	S. Guillemot, Dassault Aviation - 78, Quai Marcel Dassault, F-92214, Saint Cloud, CEDEX, France.
	Stephane.guillemot@dassault-aviation.fr

1 CODE

UEMB

1.1 Type	Euler, Multiblock
1.2 Name	UEMB
1.3 Description	Explicit, Euler multiblock code which uses structured grid within the blocks, but unstructured arrangements of blocks. Based on a steady code that uses Jameson type Runge-Kutta scheme. Cell centred. Unsteady motion is introduced using a transpiration velocity boundary condition applied at the cell centres of moving surfaces. A 2D strip theory boundary layer method is coupled to the Euler code to introduce viscous effects for some steady flow cases.
1.4 Available grid types	Structured grid within blocks, C, H and O type grids are all available.
1.5 Artificial viscosity	2^{nd} and 4^{th} order blended artificial viscosity.
1.6 Convergence acceleration techniques	None employed, although time-step constraint is relaxed for unsteady calculations.
1.7 Turbulence model	N/A
1.8 Transition model	N/A
1.9 Time-step	Local.
1.10 Convergence	Based on residuals, and C_l.
1.11 References	Ref. 13 for basis of steady code.

2 GRID

2.1 Size of grid	225,888 grid cells in 88 blocks.
2.2 Y+	N/A
2.3 Number of Surface grid points	84 X 34 = 2.856 cells
2.4 Grid type	C grid around wing
2.5 Distance of outer boundaries from the wing	10 (root) chords streamwise and normal to wing, 3 spans from wing tip in spanwise direction.
2.6 Modifications to geometry	Tip fairing is modelled, but with closure 4mm from the experimental tip.

3 RESULTS

3.1 Written Report	Euler: 152 (sections 1,3,5,7), 370 (1 & 7) Euler+boundary layer (8)
3.2 Electronic data	138, 152, 158, 191 (sections 1 – 8), 383, 193 (1,3,5,7), 370 (1 & 7)
3.3 Interpolation details	Linear interpolation in spanwise direction to measurement stations.

4 ADDITIONAL INFORMATION

4.1 Platform	Cray YMP.
4.2 CPU	
4.2.1 Total	Not given
4.2.2 per iteration	Not given
4.2.3 per cycle	Not given
4.3 Convergence	Not given

4.4 Memory	Not given
4.5 Contact for further information	M J de C Henshaw, British Aerospace (Operations) Ltd. Military Aircraft and Aerostructures, Brough, East Riding of Yorkshire, HU15 1EQ, UK. michael.henshaw@bae.co.uk

1 CODE

ENS3DAE

1.1 Type	3-D Compressible Full (not thin layer) Reynolds Averaged Navier-Stokes
1.2 Name	ENS3DAE run as Euler
1.3 Description	Beam Warming implicit central finite difference scheme. Second order accurate in space and time. Local time stepping for steady state cases.
1.4 Available grid types	Multi-block structured
1.5 Artificial viscosity	Pressure switched second/fourth order non-linear explicit with spectral radius scaling. Second order implicit
1.6 Convergence acceleration techniques	Local time stepping for steady state. Grid sequencing
1.7 Turbulence model	N/A
1.8 Transition model	N/A
1.9 Time-step	Local time stepping, CFL=4.0
1.10 Convergence	3000 iterations at M=0.90
1.11 References	Ref. 7, Ref. 8, Ref. 9

2 GRID

2.1 Size of grid	201 x 49 x 33 = 325,017 points
2.2 Y+	N/A
2.3 Number of Surface grid points	153 x 25 = 3825 points
2.4 Grid type	Single-zone C-H structured grid
2.5 Distance of outer boundaries from the wing	6 root chords forward and aft of wing. 4 root chords above and below. 4 semi-spans
2.6 Modifications to geometry	None; airfoil constant throughout span

3 RESULTS

3.1 Written Report	-
3.2 Electronic data	137, 151, 158, 168, 190 (steady only, sections 1 – 8)
3.3 Interpolation details	Linear interpolation to experimental stations

4 ADDITIONAL INFORMATION

4.1 Platform	Cray C-90 at NASA Ames, multitasked on 8 shared processors
4.2 CPU	
4.2.1 Total	Approx. 5 hrs (3000 iterations)
4.2.2 per iteration	Approx. 6 sec., 1.85 x 10-5 sec/iteration/grid point
4.2.3 per cycle	(Steady only)
4.3 Convergence	2.5 orders of magnitude on L2 norm of residual
4.4 Memory	32 million words (multitasked on 8 processors)

4.5 Contact for further information	d.m.schuster@larc.nasa.gov

NAVIER-STOKES CODES

1 CODE

	ENS3DAE
1.1 Type	3-D Compressible Full (not thin layer) Reynolds Averaged Navier-Stokes
1.2 Name	ENS3DAE
1.3 Description	Beam Warming implicit central finite difference scheme. Second order accurate in space and time. Local time stepping for steady state cases.
1.4 Available grid types	Multi-block structured
1.5 Artificial viscosity	Pressure switched second/fourth order non-linear explicit with spectral radius scaling. Second order implicit
1.6 Convergence acceleration techniques	Local time stepping for steady state. Grid sequencing
1.7 Turbulence model	Baldwin-Lomax algebraic with FMAX search limiter to force FMAX to occur in viscous layer near surface. 3-D eddy viscosity smoothing to provide spatial history effects (helpful in separated flows)
1.8 Transition model	Fully turbulent
1.9 Time-step	Local time stepping, CFL=4.0
1.10 Convergence	2000 iterations most cases, more at M=0.90
1.11 References	Ref. 7, Ref. 8, Ref. 9

2 GRID

2.1 Size of grid	201 x 49 x 41 = 403,809 points
2.2 Y+	Minimum, 3.8; maximum, 15.2; average, 7.4
2.3 Number of Surface grid points	153 x 25 = 3825 points
2.4 Grid type	Single-zone C-H structured grid
2.5 Distance of outer boundaries from the wing	6 root chords forward and aft of wing. 4 root chords above and below. 4 semi-spans
2.6 Modifications to geometry	None; airfoil constant throughout span

3 RESULTS

3.1 Written Report	137, 168 (sections 1,3,5,7)
3.2 Electronic data	137, 151, 158, 168, 190 (steady only, sections 1 – 8)
3.3 Interpolation details	Linear interpolation to experimental stations

4 ADDITIONAL INFORMATION

4.1 Platform	Cray C-90 at NASA Ames, multitasked on 8 shared processors
4.2 CPU	
4.2.1 Total	15,720 sec = 4.367 hrs (2000 iterations) CPU, 54 min Wall.
4.2.2 per iteration	7.860 sec., 1.95×10^{-5} sec/iteration/grid point
4.2.3 per cycle	(Steady only)
4.3 Convergence	2.5 orders of magnitude on L_2 norm of residual
4.4 Memory	40 million words (multitasked on 8 processors)
4.5 Contact for further information	d.m.schuster@larc.nasa.gov

CFD SOLUTIONS

CLEAN WING TEST CASES

There are 14 cases (8 steady and 6 unsteady) as detailed in Table 2, in all cases the (equilibrium) angle of attack is close to zero, and the Mach number range includes sub-critical, transonic and supersonic flow conditions. Viscous effects are comparatively insignificant for these conditions.

Solutions are presented (on the CDROM) for upper and lower surfaces at 8 spanwise stations, as specified in Table 3 (see also figure 1 of chapter 5), and sample results are plotted at a few selected conditions and spanwise locations in this chapter. A selection of convergence plots is also provided.

The reader should note that the first data point on the upper surface for sections 3 and 5 are faulty pressure points (see Ref. 2) and should not be considered in evaluations. This can be observed in figures 5 to 10, particularly Figure 10.

Run No.	Mach No.	α (deg.)	freq. (Hz)	κ	θ (deg.)	Re X10^6
Steady cases						
137	0.597	-0.005	-	-	-	4.79
138	0.597	+0.493	-	-	-	4.77
151	0.897	-0.004	-	-	-	5.79
152	0.896	+0.497	-	-	-	5.79
158	0.946	-0.004	-	-	-	5.89
168	1.093	-0.002	-	-	-	6.01
190	1.328	-0.005	-	-	-	4.07
191	1.327	+0.500	-	-	-	4.08
Unsteady cases						
383	0.597	0.004	40	0.399	0.115	4.57
370	0.896	0.001	40	0.275	0.111	5.73
160	0.947	-0.006	20	0.132	0.523	5.91
373	1.092	0.003	10	0.058	0.113	5.92
172	1.093	0.003	20	0.116	0.267	6.02
193	1.336	-0.001	40	0.198	0.222	4.10

Table 2 Flow conditions used for comparisons

Section No.	η (=y/s)	y (m)
1	0.181	0.1127
2	0.352	0.2192
3	0.512	0.3188
4	0.641	0.3991
5	0.721	0.4489
6	0.817	0.5087
7	0.875	0.5448
8	0.977	0.6082

Table 3 Spanwise measurement stations on F-5 Wing.

WING TIP

In the absence of the launcher and missile a wing tip fairing was attached to the model; this is defined in the geometry specification (see chapter 5). Three stations define the fairing, and the last of these is 4 mm short of the actual wing tip, which allows the possibility of some variation in the modelling of the geometry. CFD results generated within this benchmark exercise have indicated that minor compromises to the geometry in this region are insignificant compared to changes in grid density and/or model physics. Indeed a linear extrapolation of the wing section to the full span with a simple closure at the tip is a reasonable compromise of the actual geometry.

Overall the codes UEMB and EUL3DU were found to give almost identical results, the main differences being due only to the grid density (particularly around the leading edge). The tip geometry was defined differently in these two sets of results; for UEMB the fairing definition (three stations) is used, but the last (undefined) 4-mm are truncated and the tip closed with a flat surface. In the EUL3DU geometry, on the other hand, the tip is modelled by extending the constant wing section to the tip, which is located at 0.6476 m. Thus the wing has the span of the tested wing, but the change in shape of the fairing is not modelled at all. The tip is closed by collapsing the grid to a plane in a section located about 13 mm from the tip, which actually gives additional span to the wing.

The Cp distribution at station 8 (97.7%) is shown in Figure 2, for run 152 (M=0.896, α=0.497°).

On the lower surface the EUL3DU results show sharper and earlier peak suction than the UEMB results, but this is explained by the difference in mesh density. In fact the EUL3DU grid has 160 chordwise points compared to 84 for the UEMB grid. Overall the EUL3DU lower surface results agree more closely with the experimental points. On the upper surface this position is somewhat reversed, with the UEMB results closer to the experimental points. Once again the grid density is seen to make a difference, manifested by the sharpness of the shock wave.

For information, an UEMB result obtained using viscous coupling is also plotted. This shows closer agreement in terms of shock position and peak pressures on the upper surface, the difference is less pronounced on the lower surface. Although the results with the two geometry definitions show variation, these variations appear to be associated with different grid density rather than differences in the geometry definition per se. Overall, it is concluded that the Cp variations, due to these differences in tip geometry modelling, are not significant.

CONVERGENCE

There is some variation in the metrics used by the different methods to monitor convergence, the metric(s) used by each method are noted in the formulary above. For information the convergence for a sample of codes is plotted for two of the run conditions run 152 (steady) and run 172 (unsteady) in Figure 3 (Full potential) and Figure 4 (Euler). These are typical plots and will inform the reader of the general level of convergence that has been achieved for the results presented herein.

STEADY SOLUTIONS

Steady solutions are presented as sectional Cp plots at spanwise stations 1, 3, 5, 7 for a selection of the flow conditions, and data for all stations and all the steady conditions specified in Table 2 are available on the accompanying CDROM. The reader is invited to plot these data for the purposes of more extensive comparison. Code to code comparisons are made for the transonic case, run 152, in Figure 5 (UTSP and Full Potential) and Figure 6 (Euler and Navier-Stokes). For clarity a reduced set of results which compare the four different levels of approximation are shown in Figure 7 (run 137, subsonic), Figure 8 (run 152, transonic) and Figure 10 (run 168, supersonic).

The various methods are in *overall* agreement, but differ somewhat in detail. The inboard pressures tend to be overpredicted by all the methods, but this is almost certainly due to the sidewall boundary layer affecting the experimental results. The tip pressure detail is sensitive to spanwise grid clustering, and it is suggested that this is as significant as the changes in tip geometry mentioned above.

At Mach numbers near 0.9, and above, a leading edge shock appears, and this is somewhat sensitive to the grid spacing around the leading edge for the inviscid methods. For Navier-Stokes methods particular attention to cell clustering in this region may be required, and it is not clear whether the flow near the leading edge should be laminar or turbulent.

The two UTSP methods show fairly close agreement (Figure 5), although UTSPV21 fails to capture the leading edge peak pressure (lower surface) and the sharpness of the shock (upper surface); this is due to the differences in grid fineness. CAP-ASP uses more than twice as many chordwise grid points, and this indicates that of the order of 90 (on each surface) are required. It may be noted that the shock is further aft for CAP-ASP, particularly at the tip, however, this agrees well with the EUL3DU (Euler) predicted position (Figure 8) and other fine grid Euler results (Ref. 11). Both Full Potential methods capture the leading edge peak better than the UTSP results.

There is a significant difference in the shock position between the two Full Potential methods. HELIFP and TCITRON use similar grid densities (although HELIFP uses more spanwise stations) and the difference is attributed to the different formulations: HELIFP is a conservative formulation and TCITRON is non-conservative.

The difference in shock position for the Euler methods UEMB and EUL3DU (Figure 6) is once again entirely attributable to the different grid densities, however, the difference between PMB3D and UEMB is less easily explained, as these methods were run on the same grid. The implicit formulation (PMB3D) in fact shows closest agreement with EUGENIE, an unstructured grid code that in this case is used with boundary layer coupling to model the effects of viscosity. Figure 9 shows a comparison between UEMB and EUGENIE (i.e. structured and unstructured grids respectively) both run in Euler and Euler with viscous coupling mode. There appears to be no significant difference between the grid technologies, and the inclusion of viscous coupling achieves the correct shock position in both cases.

For the subsonic case (Figure 7) there is virtually no difference between the various levels of approximation, although the trailing edge treatment for the codes results in some differences in pressure. The two methods that include viscosity (RANS code ENS3DAE and EUGENIE with boundary layer coupling) show a similar trend in Cp at the trailing edge. For the supersonic case there is again variation in the trailing edge treatment, although overall the various levels of approximation appear to agree well. Euler with boundary layer coupling (EUGENIE) matches most closely to experiment, and the Full Potential method shows the least agreement with other methods or experiment.

UNSTEADY SOLUTIONS

Unsteady solutions are presented as sectional plots of the real and imaginary parts of the pressure coefficient (CpReal and CpImag) at spanwise stations 1 and 7 for a selection of flow conditions. Data for all the stations and all the unsteady flow conditions specified in Table 2 are available on the accompanying CDROM. The reader is invited to plot these data for the purposes of more extensive comparison.

Code to code comparisons are presented for run 370 (transonic) in Figure 11 (UTSP and Full Potential) and Figure 12 (Euler). A reduced set of results which compare the three different levels of approximation are shown in Figure 13 (run 383, subsonic), Figure 14 (run 370, transonic), and Figure 15 (run 373, supersonic).

The reader should note that the first experimental point on section 1, upper surface, for run 370 appears to be in error; although no error has been identified in the experimental dataset for this point. The point is not included in the plots reported here (e.g. Figure 11), although it remains in the experimental data included on the CDROM.

Only one set of UTSP data is available (UTSPV21, run 370, Figure 11) and this underestimates the peaks in the real and imaginary pressures. As before this is due to the coarseness of the mesh used in this code. The Full Potential codes show reasonable agreement with each other, although the position of the peak in CpImag agrees less well on the outboard stations. HELIFP (with conservative formulation) appears to match experiment most closely for this case. The Euler methods also show reasonable agreement with each other (Figure 12) although the EUL3DU method tends to predict larger outboard peaks for both real and imaginary parts. Overall, EUGENIE matches most closely to the experimental values.

The predictions for subsonic and supersonic flow show fairly close agreement between all the methods (Figure 13 and Figure 15), although the outboard peak Cp (real and imaginary) is rather reduced for the Full Potential code at supersonic conditions.

No differences in the results are attributed to differences in the way that unsteady motion is introduced (e.g. transpiration boundary conditions or mesh movement), however, the oscillation amplitude is comparatively small for this test case.

COMPLEX CONFIGURATION TEST CASES

The F-5 test series includes a range of geometries, increasing in complexity from the clean wing to the wing with stores and attendant components, as defined in chapter 5, tables 3 and 4. Computational solutions are presented for the geometry described by table 3d, of chapter 5, i.e. F-5 wing with tip launcher + missile body + aft fins + canard fins, at the flow conditions specified in Table 4.

RUN	MACH	κ	α	Re	F	θ
Steady Cases						
320	.897	0	-.000	5.65	-	-
Unsteady Cases						
348	.595	.401	.004	4.62	40.000	.111
352	.897	.069	-.002	5.73	10.000	.115
355	.896	.275	.004	5.73	40.000	.117
302	1.327	.199	.016	4.20	40.000	.221

Table 4 Wing With Tip Launcher + Missile Body + Aft Fins + Canard Fins

The Euler methods UEMB (structured) and EUGENIE (unstructured) have provided results for the complex configurations, the grids were as follows: -

UEMB: Multiblock: 290 blocks, 238,263 cells (11,712 surface cells).

EUGENIE: 120,307 grid nodes (6,770 surface nodes)

Although there is an increase in the number of grid points, compared to the number for the clean wing, in both cases the increase is comparatively modest compared to the increase in complexity of the geometry. This is especially true of the structured code (UEMB), where some compromise in surface density has been necessary to minimise the number of cells used. The grids are illustrated in plots provided on the CDROM (in directory 'Grids')

STEADY SOLUTIONS

Results are presented for steady flow case, run 320, in the form of Cp maps only. The plots may be viewed from the CDROM in directory Chapter4/ComplexWing/Steady/Run320, and are in postscript form. Detailed Cp plots of the missile, calculated using EUGENIE, are given in EU_EUGENIE_SURF and EU_EUGENIE_SURFZ (an enlargement of the aft fins area). The results for EUGENIE and UEMB are compared in EU_EUGENIE_UEMB_XCUT (field plot) and EU_EUGENIE_UEMB_WING (wing surface). For these figures the reader should note that EUGENIE is equivalent to the DAv label, and UEMB to the BAe label. The agreement between the two methods appears to be good for this steady flow condition.

UNSTEADY SOLUTIONS

Sectional plots are provided at sections 1, 3, 7, and 8 (Table 3) for the real and imaginary components of the pressure coefficient for the cases defined in Table 4. Plots for the three cases with pitch frequency of 40 Hz are included below. The agreement of the codes, and with experiment, is close for the subsonic and supersonic flow conditions for the real component of Cp (Figure 16 and Figure 20), but less good for the imaginary Cps. EUGENIE appears to underestimate Cp compared to experiment, whereas UEMB achieves fairly good agreement except at the outermost section (Figure 17and Figure 21). For the transonic flow case (run 355) the codes show a basic agreement in trend, but differ in detail (Figure 18 and Figure 19), however, the agreement with experiment is less well determined, especially at the outboard stations. The peaks in CpReal and Cplmag, identified by the codes (which exhibit the same trends) are not present at the measurement locations of the experimental results.

DATA LAYOUT

The data relevant to this chapter is held in directories chapter4 and chapter5 (experimental). The structure for the CFD data (chapter 4) is shown in Figure 1.

The location of results for particular runs is self-evident from the structure of the chapter directory tree. Each RUN*** directory contains all the CFD results for that particular run number (see Table 2 and Table 4) with a designation according to the following key: -

MM_CCCC_SS

Where MM is the method identifier, CCCC is the code identifier, and SS the section number.

UT	UTSPV21	S1
FP	CAPASP	S2
EU	HELIFP	S3
NS	TCITRON	S4
	EUL3DU	S5
	PMB3D	S6
	EUGENIE	S7
	EUGENIE + BL	S8
	UEMB	
	ENS3DAE	

For example, section 5 of data for run 151 using the code EUL3DU has the code EU_ EUL3DU_S5 and held in directory RUN151.

Some RUN*** directories also contain a directory entitled 'Plotting', and this contains files for producing the plots printed below, with one or two additional cases for further information. To produce plots execute Xmgr.xxx_sh, this uses the corresponding set.xxx and graph.uCp files. Ensure that the directory is correctly set in Xmgr.xxx_sh by modifying the 'DIR=' line appropriately. Different sections may be plotted using the scripts, by editting the filenames in Xmgr.xxx_sh.

Postscript files illustrating some of the grids used in this exercise are provided in the directory 'Grids'

Two movie files are provided for the clean wing unsteady case, run160, these are both generated from results from the EUGENIE code. The first 'skin.mov' shows the upper surface shaded according to Cp value through two pitch cycles, the second ('profil.mov') shows the Cp plot at a section at 0.535 m span as it pitches through two cycles.

A full list of contents is given in the README file.

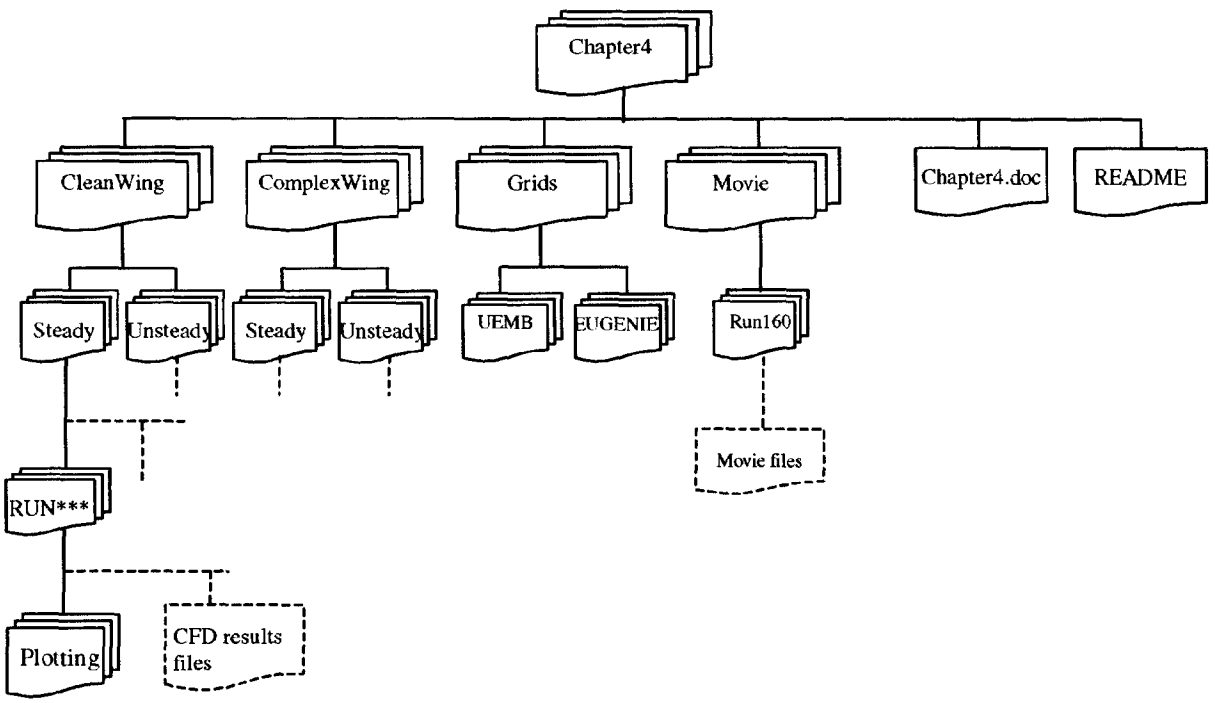

Figure 1 Directory structure for Chapter 4 on CDROM.

a)

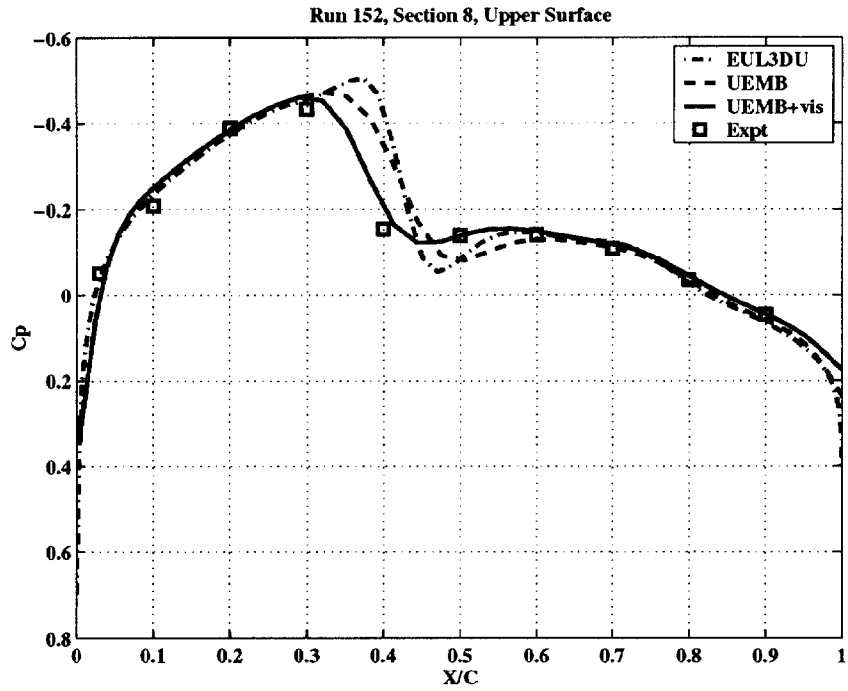

b)

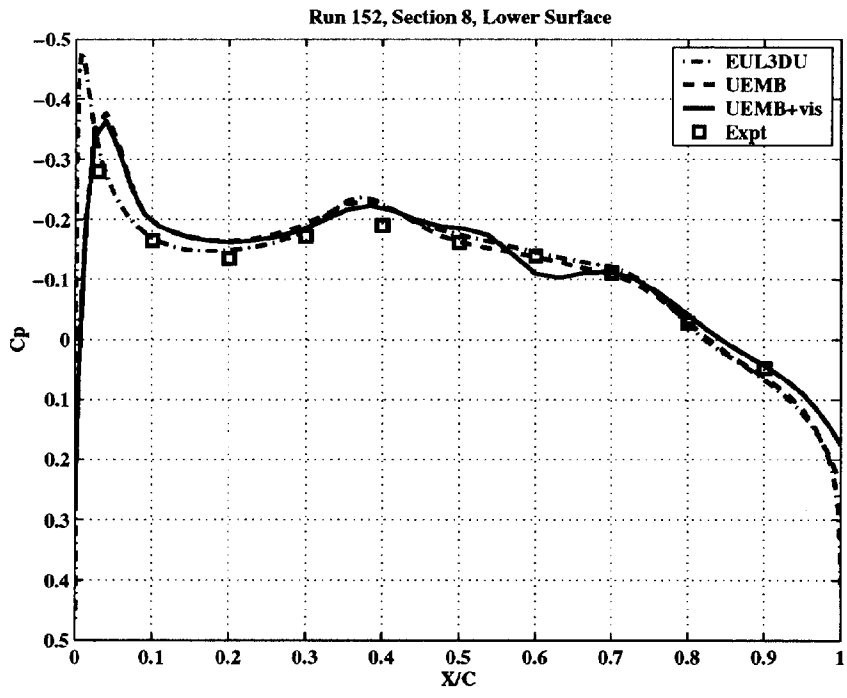

Figure 2 **Comparison of EUL3DU and UEMB at section 8 for run 152. Cp is plotted for a) upper surface, and b) lower surface. This figure shows that different tip modelling has less effect than other factors (such as inclusion of viscosity, designated UEMB+vis)**

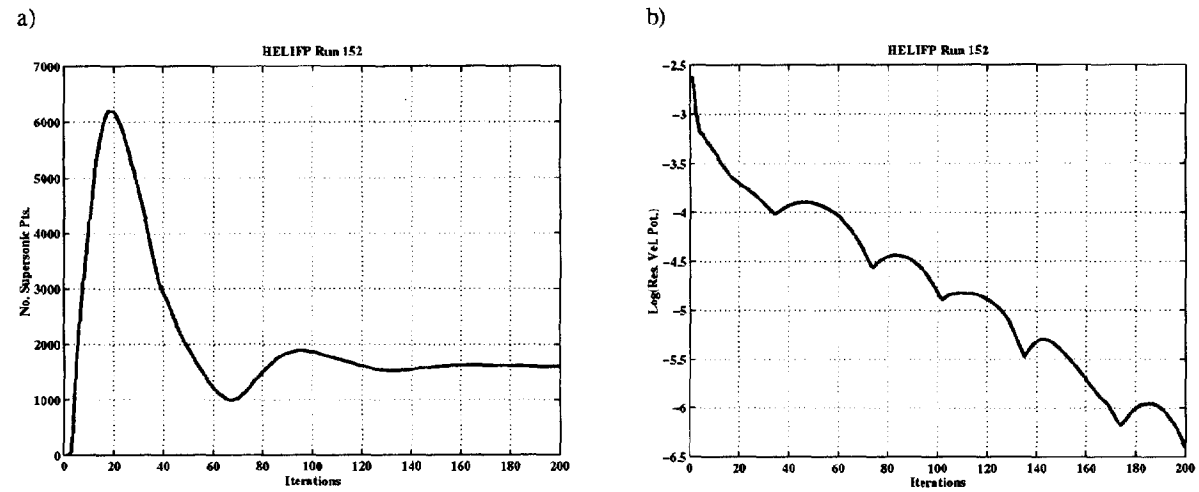

Figure 3 Convergence plots for Full Potential methods. Convergence for the code HELIFP is illustrated for run 152. a) Number of supersonic points plotted against iteration number, b) residual of velocity potential plotted against iteration number.

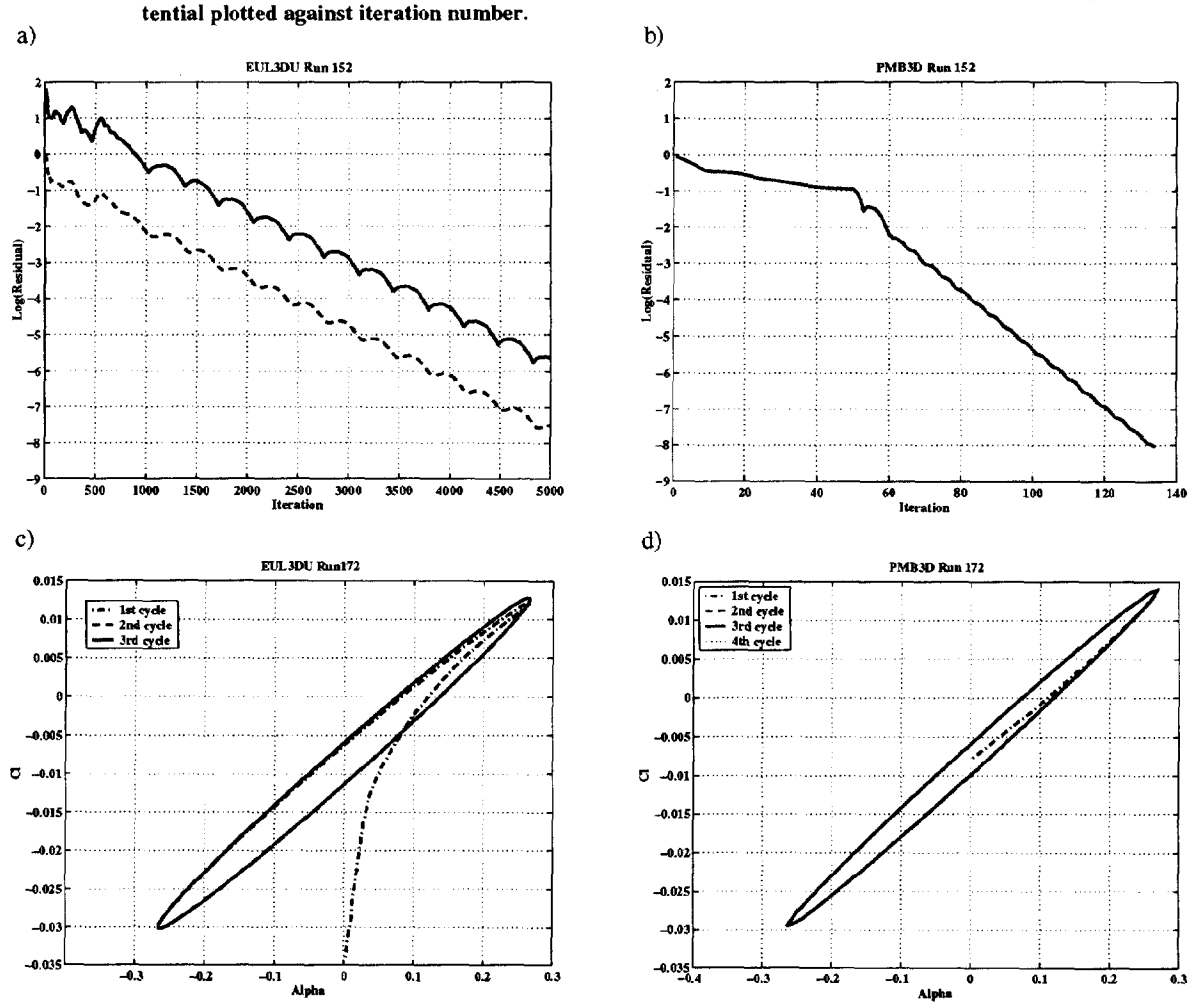

Figure 4 Convergence plots for Euler methods. Explicit (EUL3DU) and implicit (PMB3DU) algorithms are illustrated. a) EUL3DU for run 152 (steady), residual vs. iteration; b) PMB3D for run 152 (steady), residual vs. iteration; c) EUL3DU for run 172 (unsteady), Cl vs. α for 3 pitch oscillations; d) PMB3D for run 172 (unsteady), Cl vs. α for 3.25 pitch oscillations.

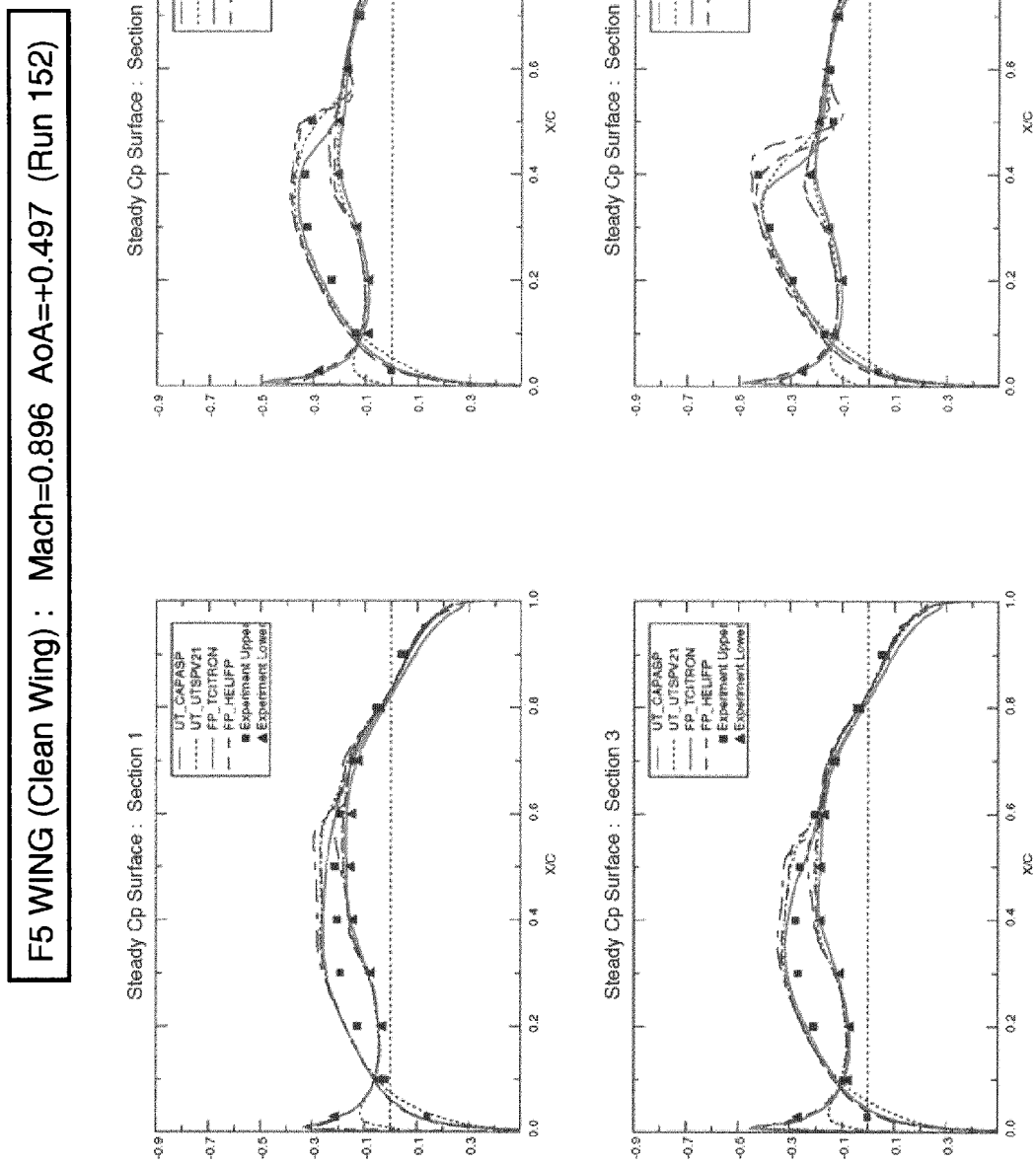

Figure 5 **Code comparisons, steady flow. Run 152 (M=0.896, α=0.497°), Cp vs. X/C for UTSP and Full Potential codes (UTSPV21, CAP-ASP, TCITRON and HELIFP) at sections 1, 3, 5, and 7.**

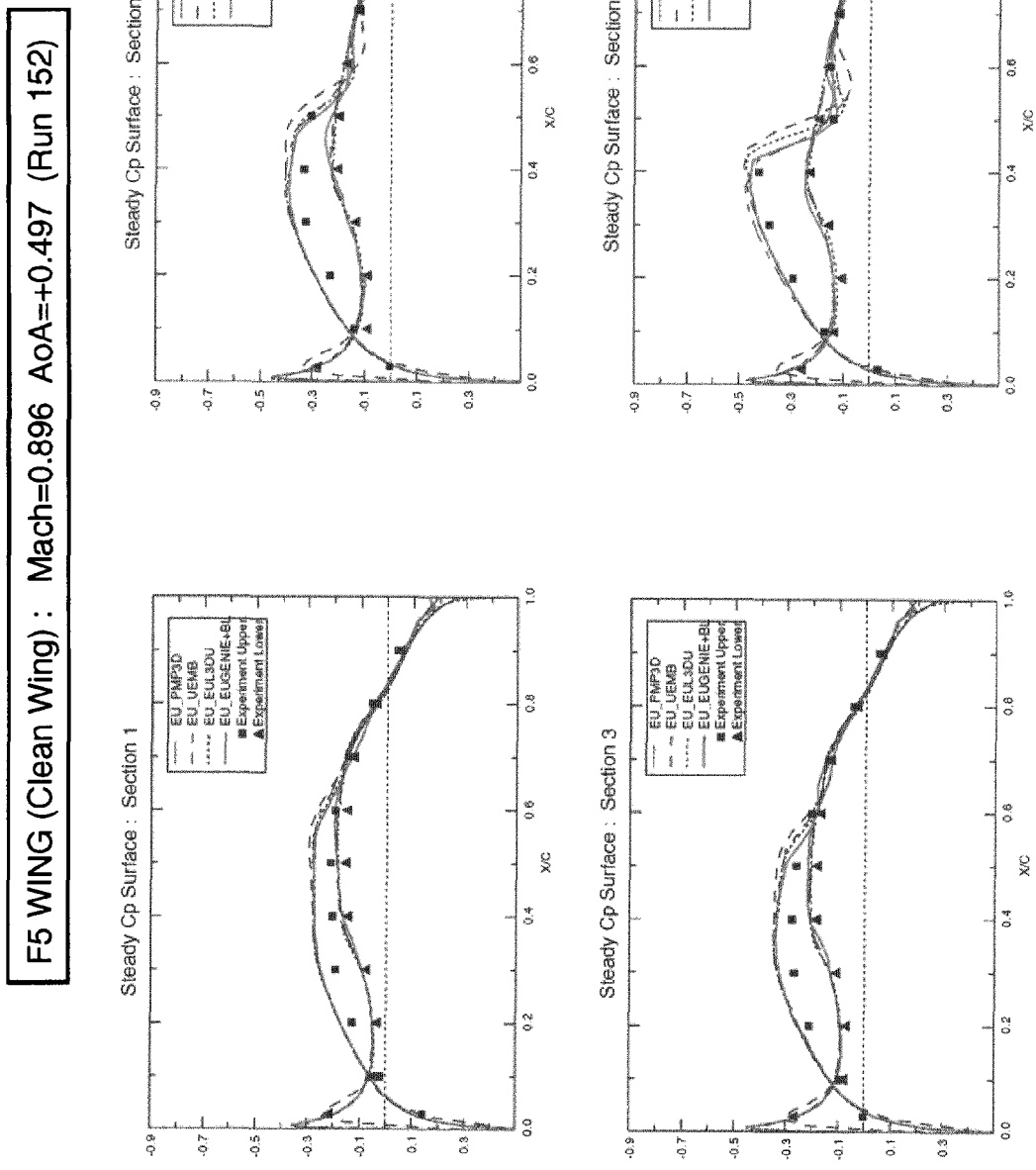

Figure 6 **Code comparisons, steady flow. Run 152 (M=0.896, α=0.497°), Cp vs. X/C for Euler codes (PMB3D, UEMB, EUL3DU and EUGENIE) at sections 1, 3, 5, and 7. Note that for viscous effects are included in EUGENIE through boundary layer coupling.**

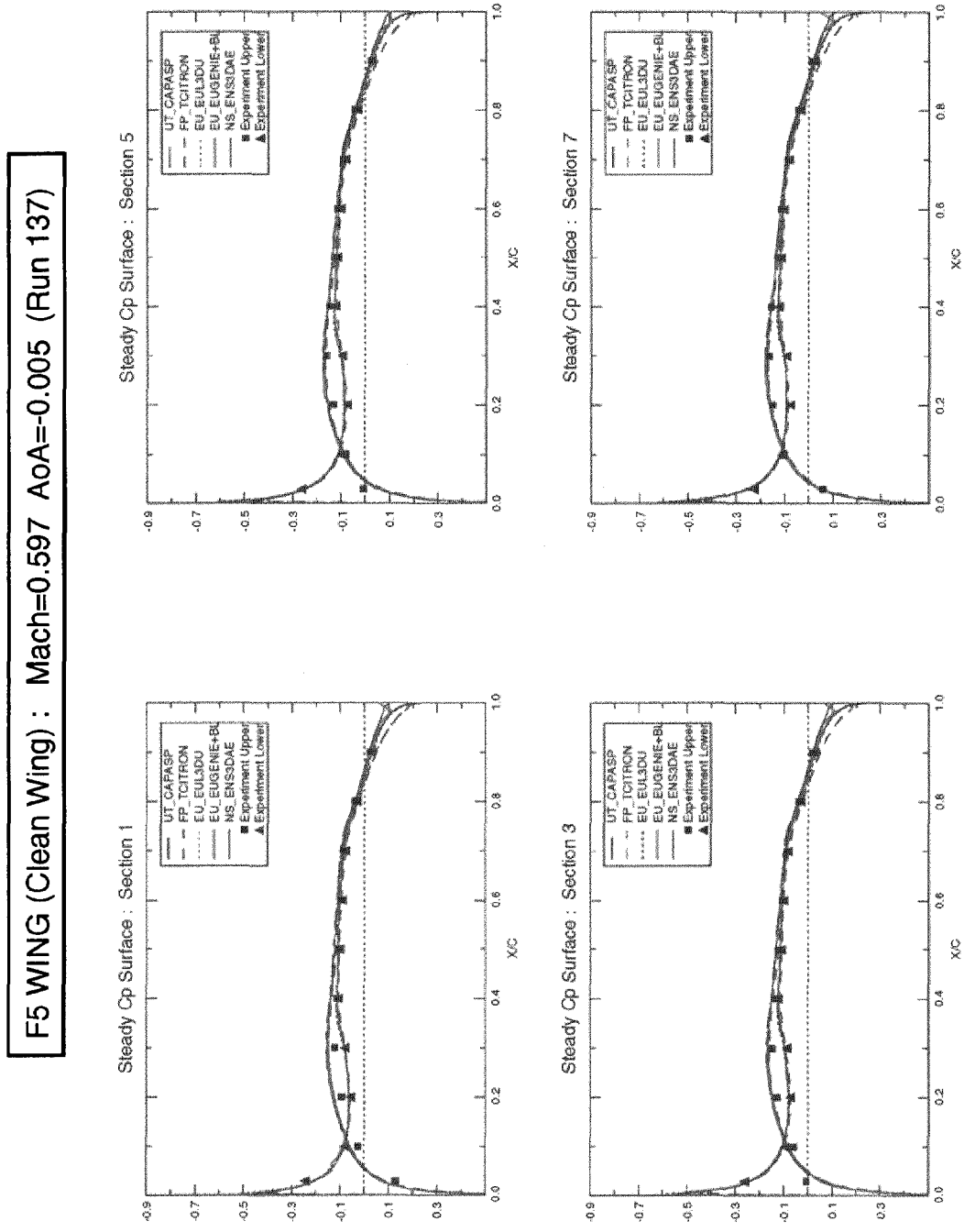

Figure 7 **Method comparisons, steady flow. Run 137 (M=0.597, α=-0.005°), Cp vs. X/C for a selection of UTSP, Full Potential, Euler and Navier-Stokes methods at sections 1, 3, 5, and 7. Note that viscous effects are also introduced into EUGENIE through boundary layer coupling.**

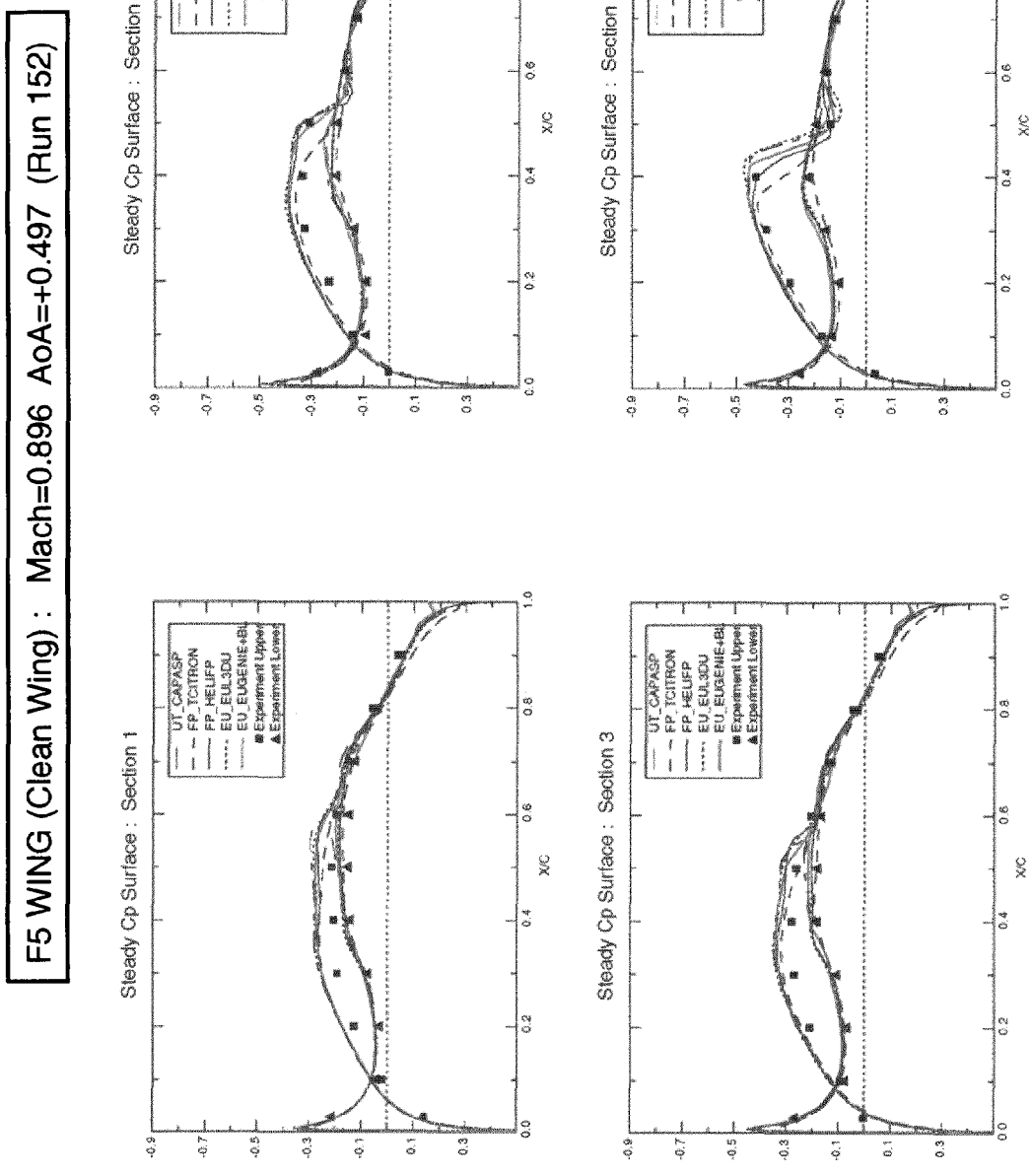

Figure 8 **Method comparisons, steady flow. Run 152 (M=0.896, α=+0.497°), Cp vs. X/C for UTSP, Full Potential and Euler methods at sections 1,3, 5, and 7. Note that EUGENIE includes viscous effects through boundary layer coupling.**

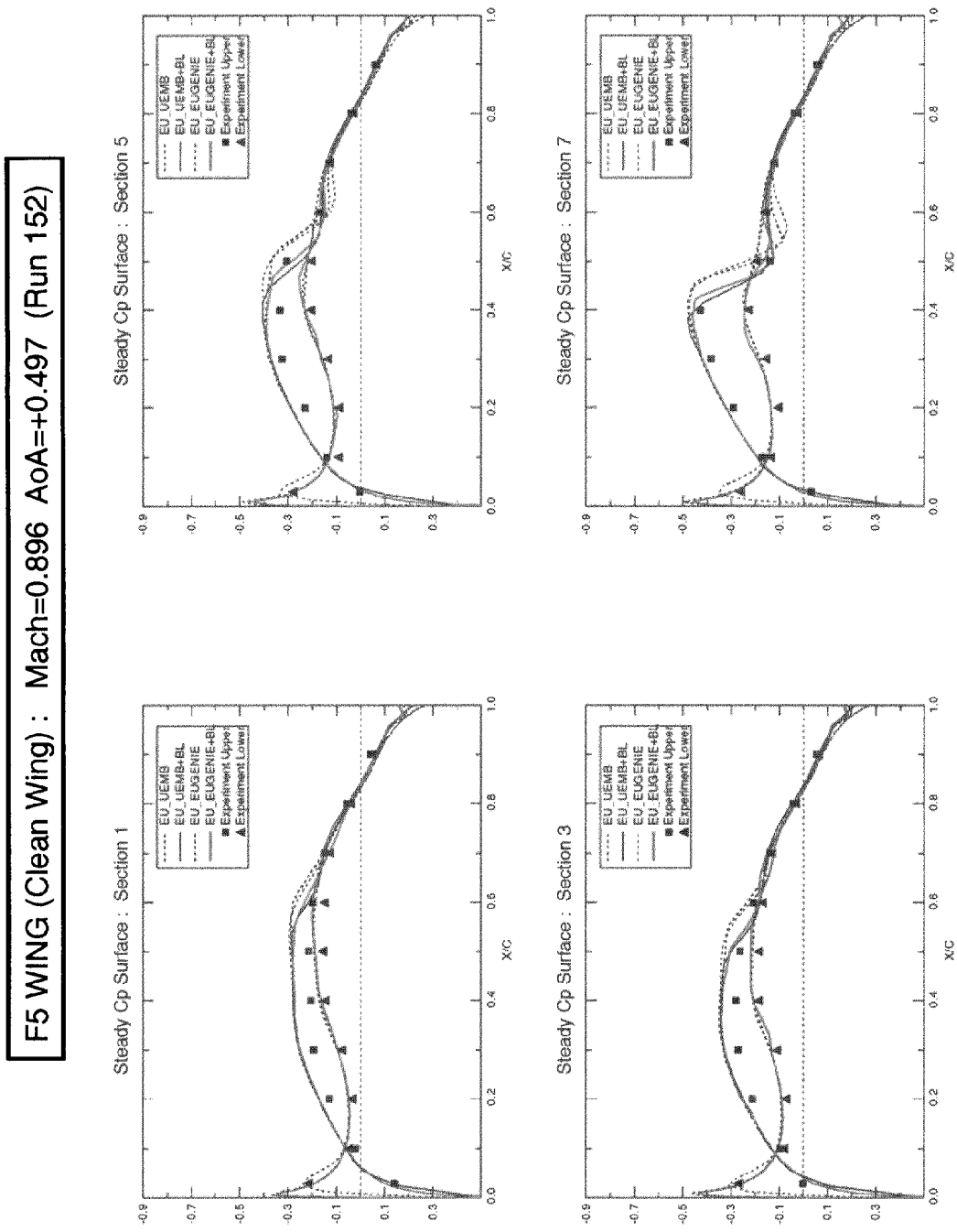

Figure 9 **Code Comparison, steady flow. Run 152 (M=0.896, α=+0.497°), Cp vs. X/C at sections 1, 3, 5 and 7. Euler methods with and without viscous coupling. UEMB (Structured) and EUGENIE (Unstructured).**

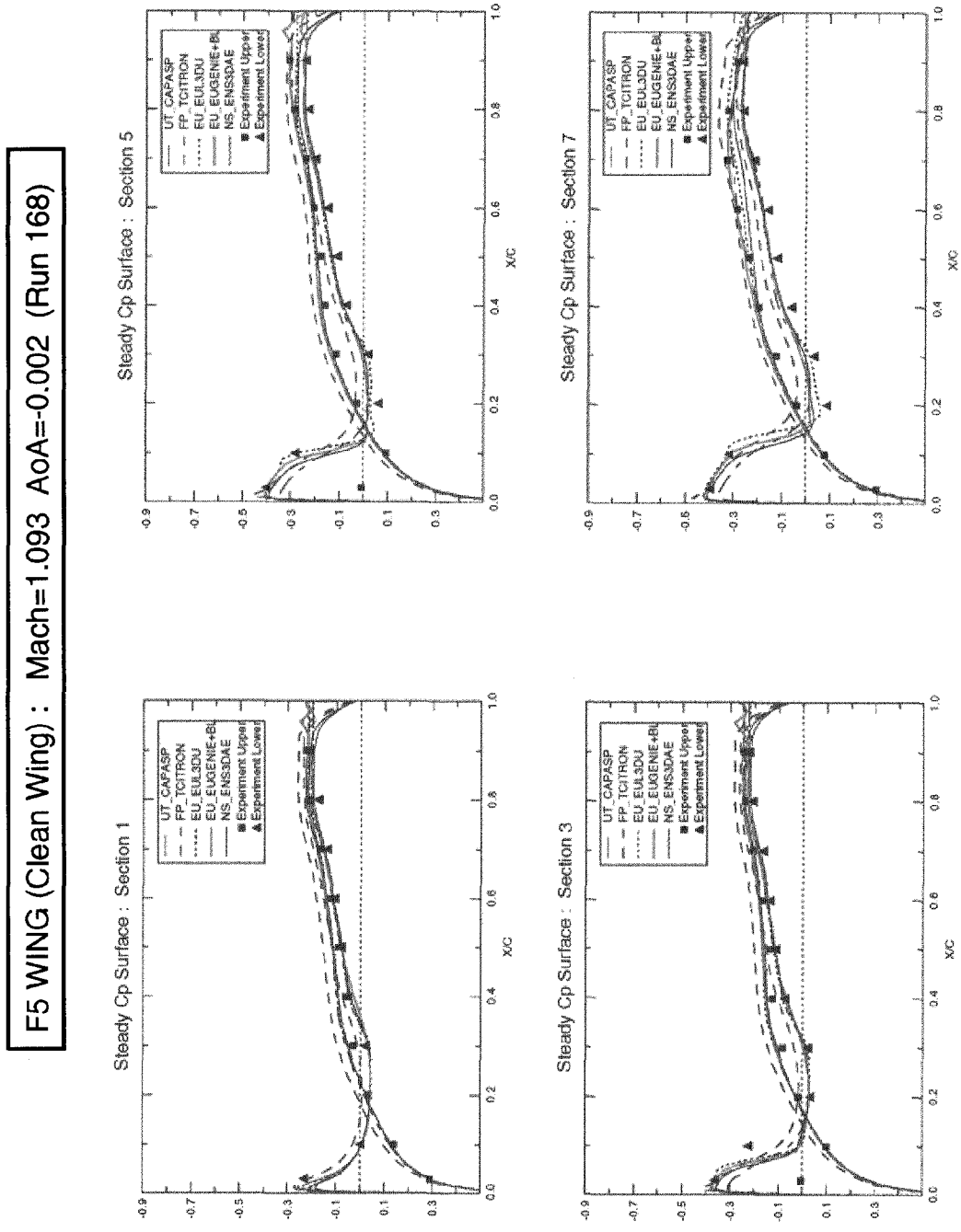

Figure 10 **Method comparisons, steady flow. Run 168 (M=1.093, α=-0.002°), Cp vs. X/C for UTSP, Full Potential, Euler and Navier-Stokes codes at sections 1, 3, 5, and 7. Note that EUGENIE includes viscous effects through boundary layer coupling.**

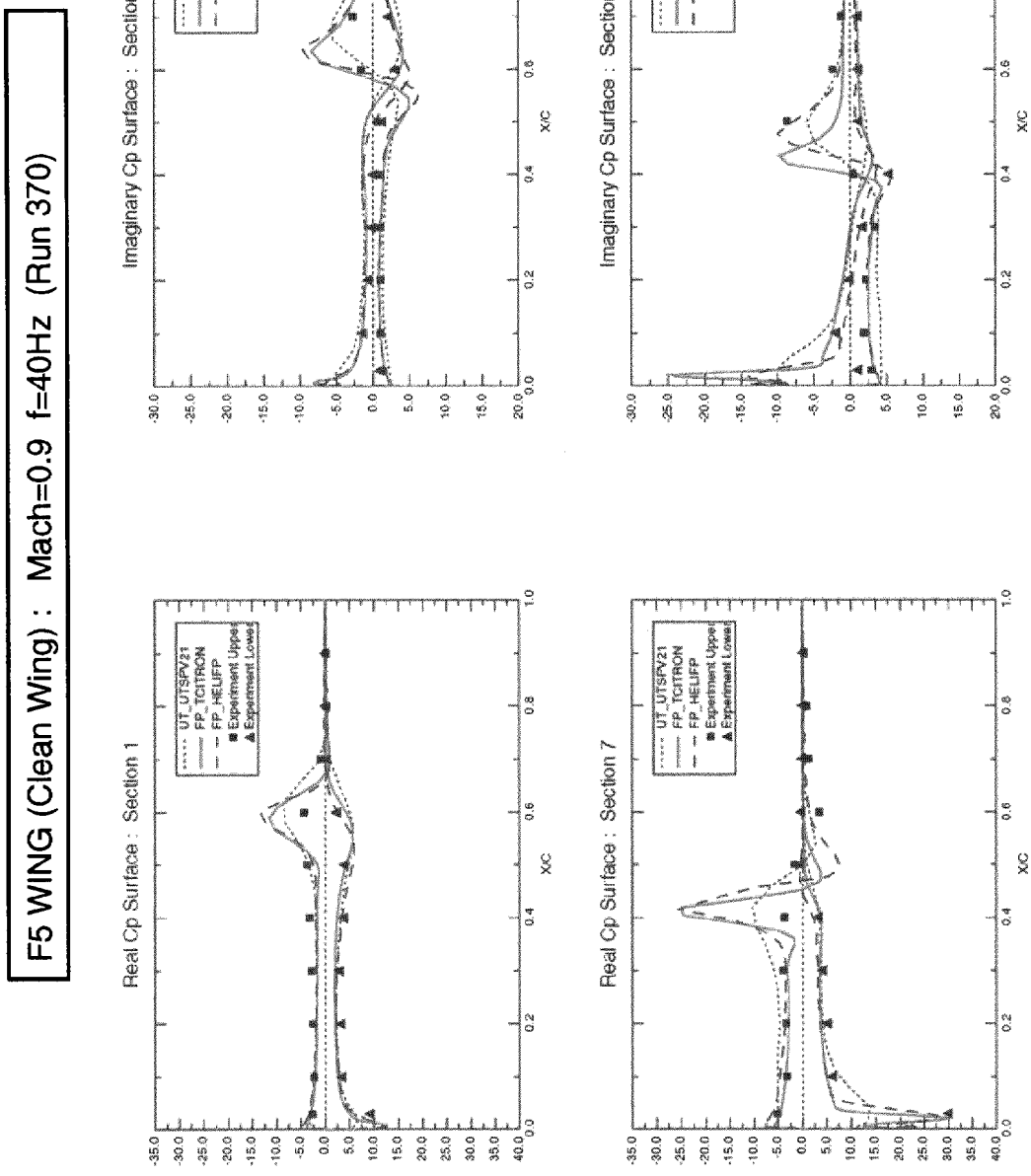

Figure 11 **Code comparisons, unsteady flow. Run 370 (M=0.896, α=0.001°, F=40 Hz, θ=0.111°), CpReal and CpImag vs. X/C for UTSP and Full Potential codes (UTSPV21, TCITRON AND HELIFP) at sections 1 and 7.**

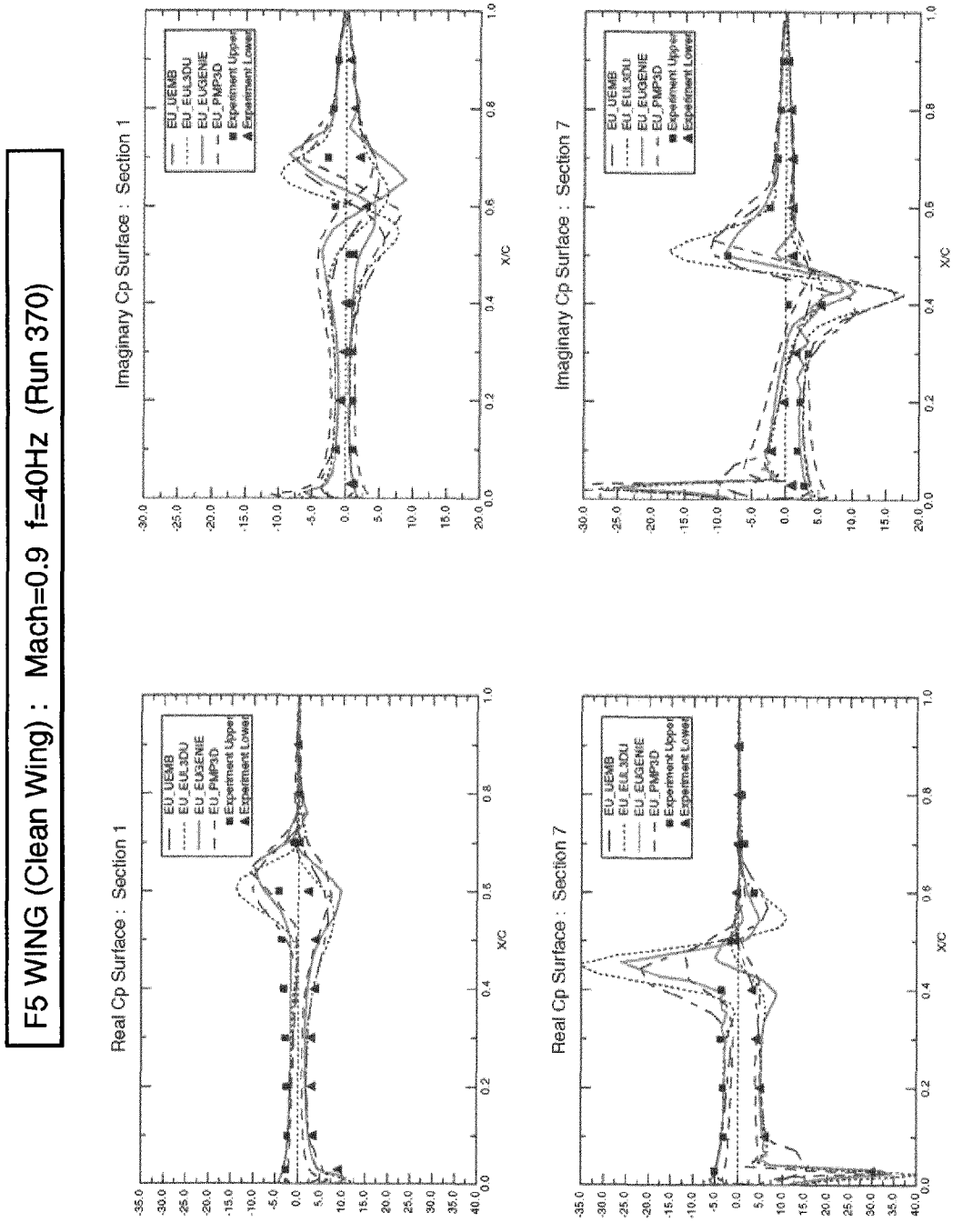

Figure 12 **Code comparisons, unsteady flow. Run 370 (M=0.896, α=0.001°, F=40 Hz, θ=0.111°), CpReal and CpImag vs. X/C for Euler codes (UEMB, EUL3DU, EUGENIE, and PMB3D) at sections 1 and 7.**

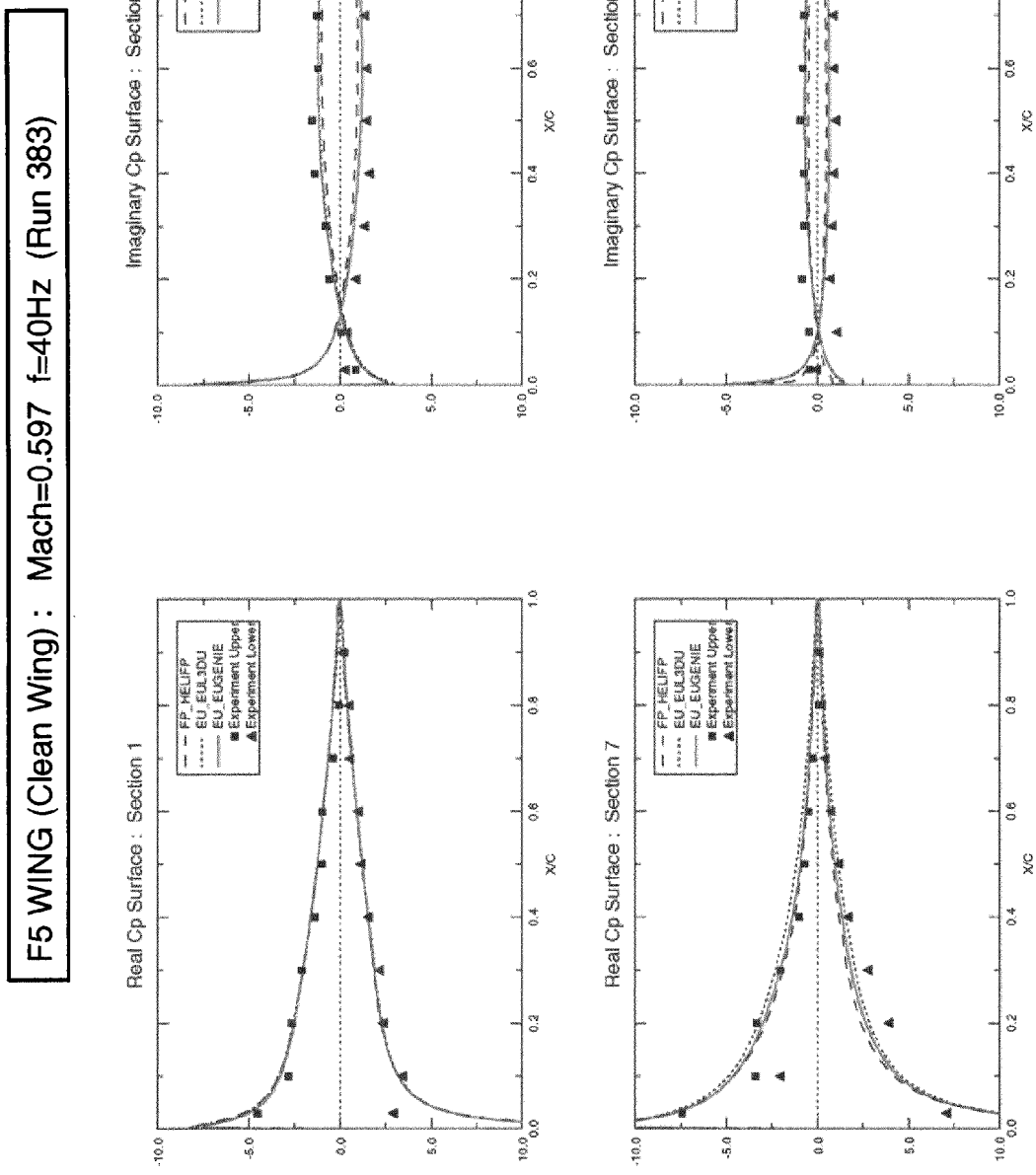

Figure 13 **Method comparisons, unsteady flow. Run 383 (M=0.597, α=0.004°, F=40 Hz, θ=0.399°), CpReal and CpImag vs. X/C for Full Potential and Euler methods at sections 1 and 7.**

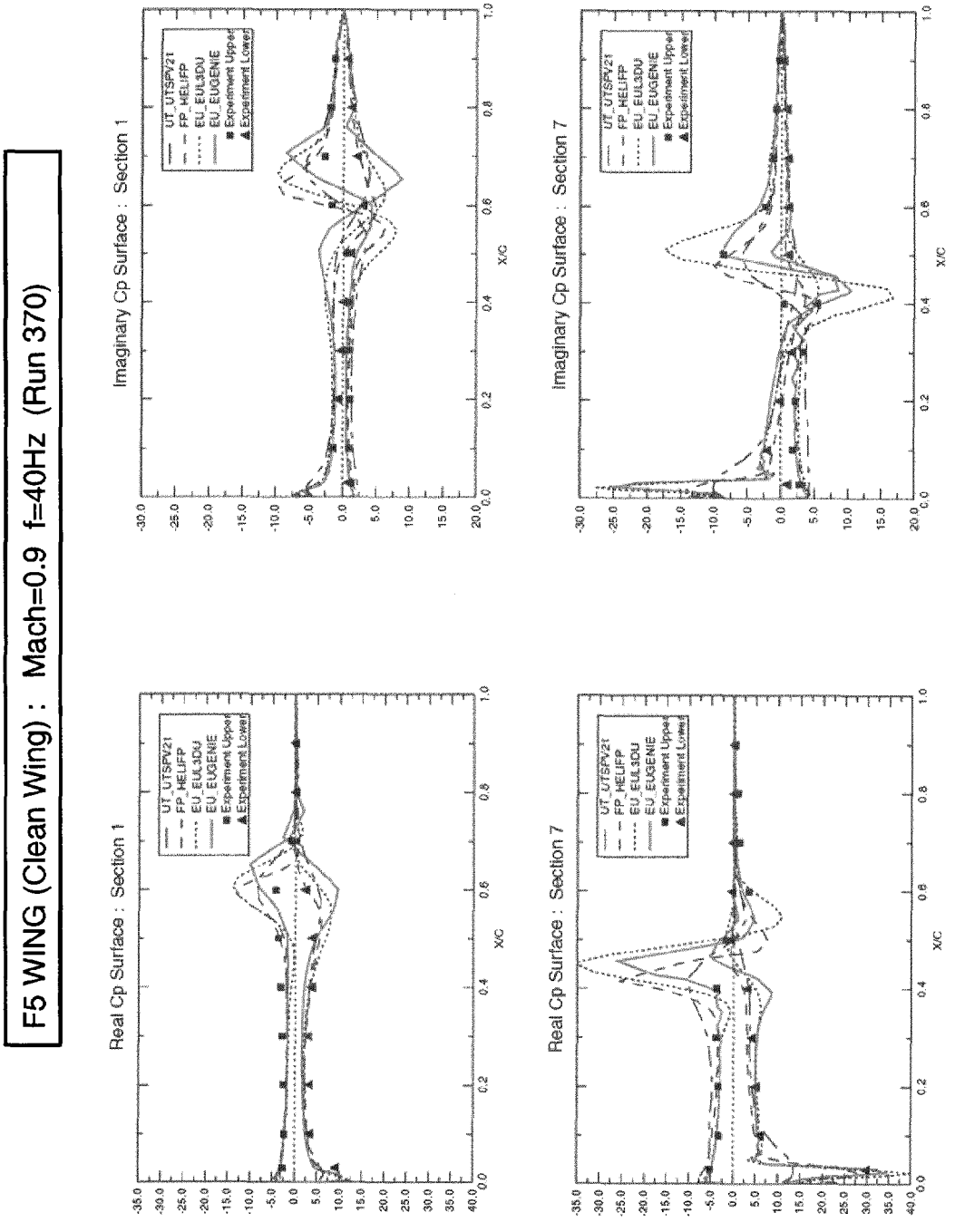

Figure 14 **Method comparisons, unsteady flow. Run 370 (M=0.896, α=0.001°, F=40 Hz, θ=0.275°), CpReal and CpImag vs. X/C for UTSP, Full Potential and Euler codes at sections 1 and 7.**

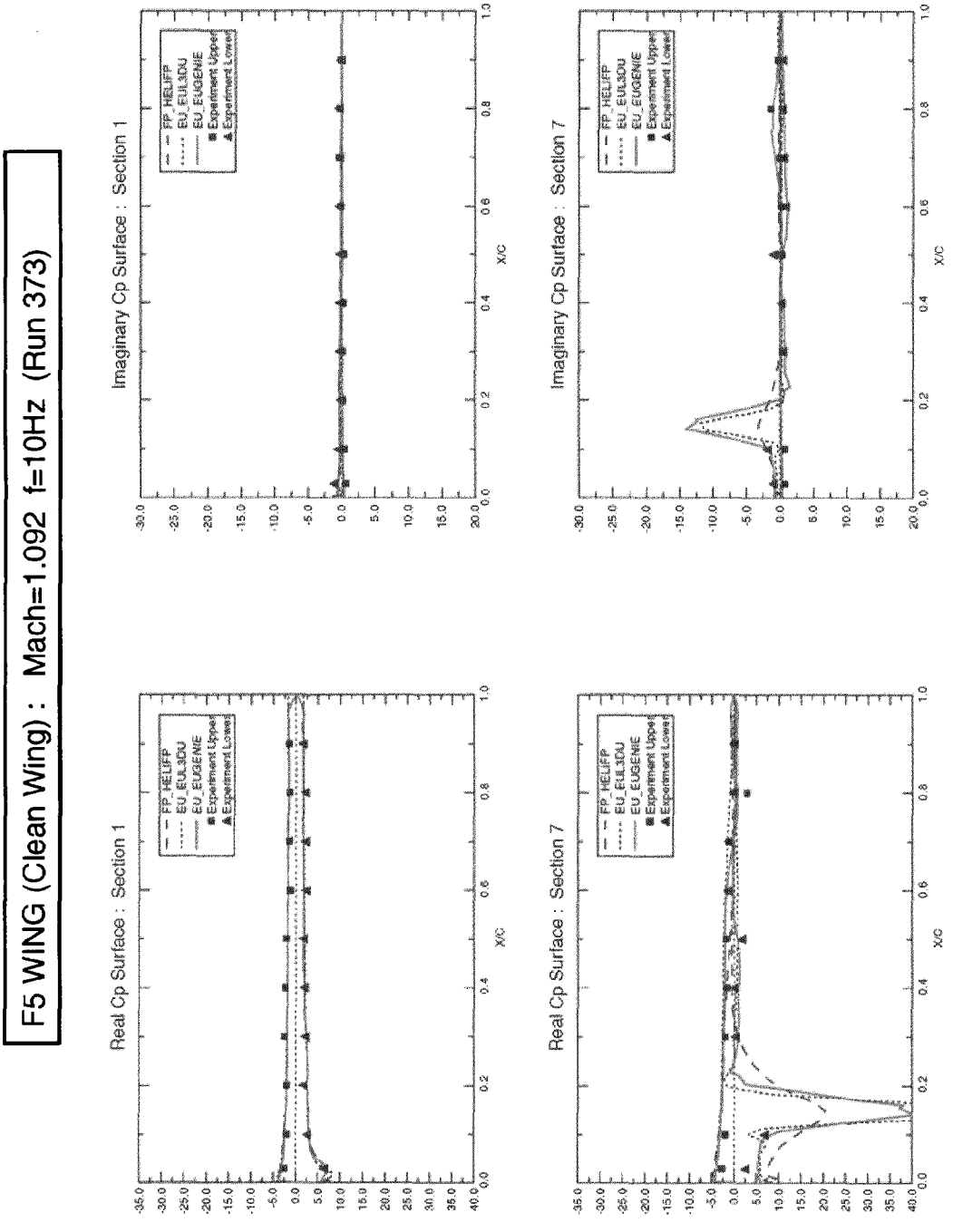

Figure 15 **Method comparisons, unsteady flow. Run 373 (M=1.092, α=0.003°, F=10 Hz, θ=0.058°), CpReal and CpImag vs. X/C for Full Potential and Euler codes at sections 1 and 7.**

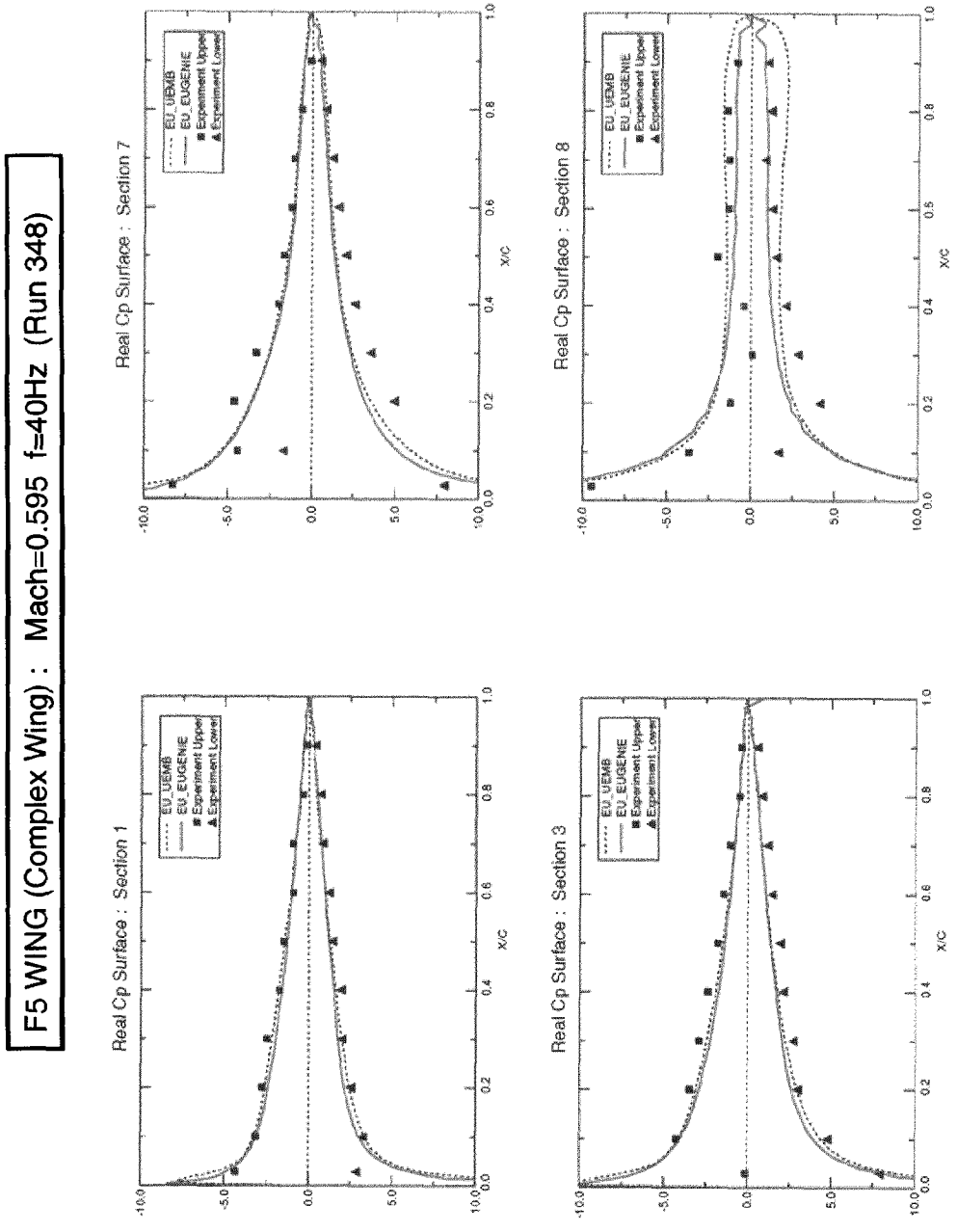

Figure 16 **Code Comparison, unsteady flow. Run 348 (complex geometry, M=0.595, F=40 Hz, α=0.004°, θ=0.111°), CpReal vs. X/C for Euler methods (EUGENIE and UEMB) at sections 1,3,7 and 8.**

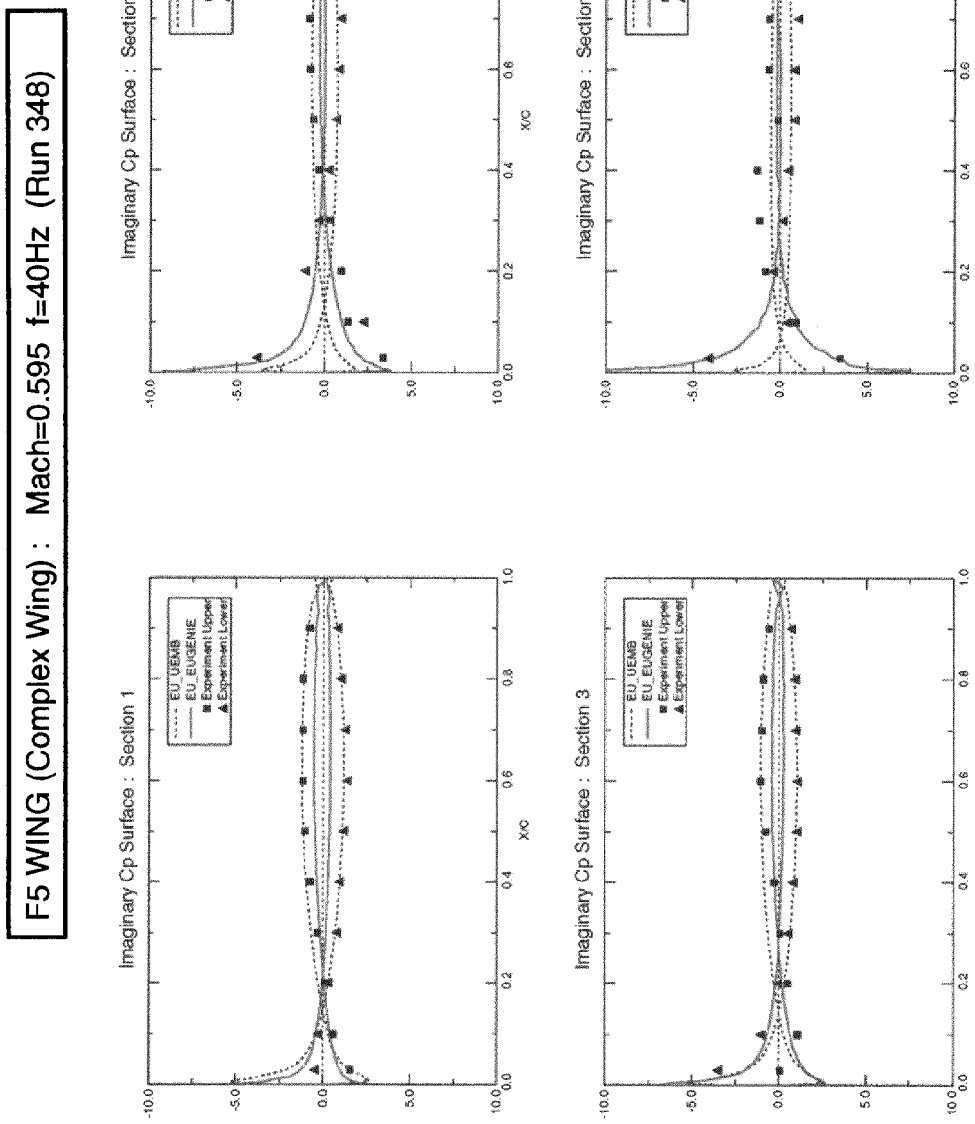

Figure 17 **Method Comparison, unsteady flow. Run 348 (complex geometry, M=0.595, F=40 Hz, α=0.004°, θ=0.111°), CpImag vs. X/C for Euler methods (EUGENIE and UEMB) at sections 1, 3, 7 and 8.**

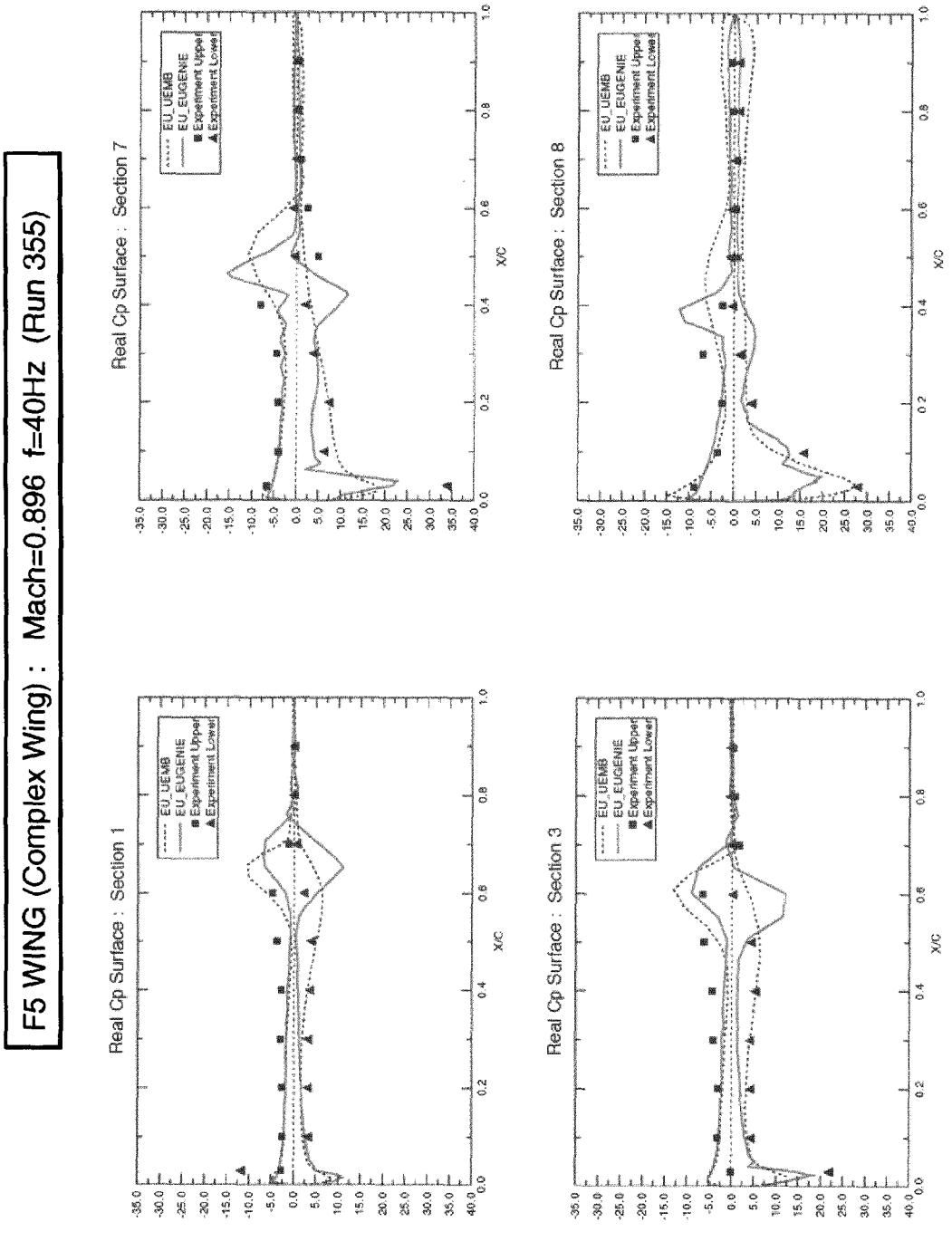

Figure 18 **Code Comparison, unsteady flow. Run 355 (complex geometry, M=0.869, F=40 Hz, α=0.004°,θ=0.117°) CpReal vs. X/C for Euler methods (EUGENIE and UEMB) at sections 1, 3, 7 and 8.**

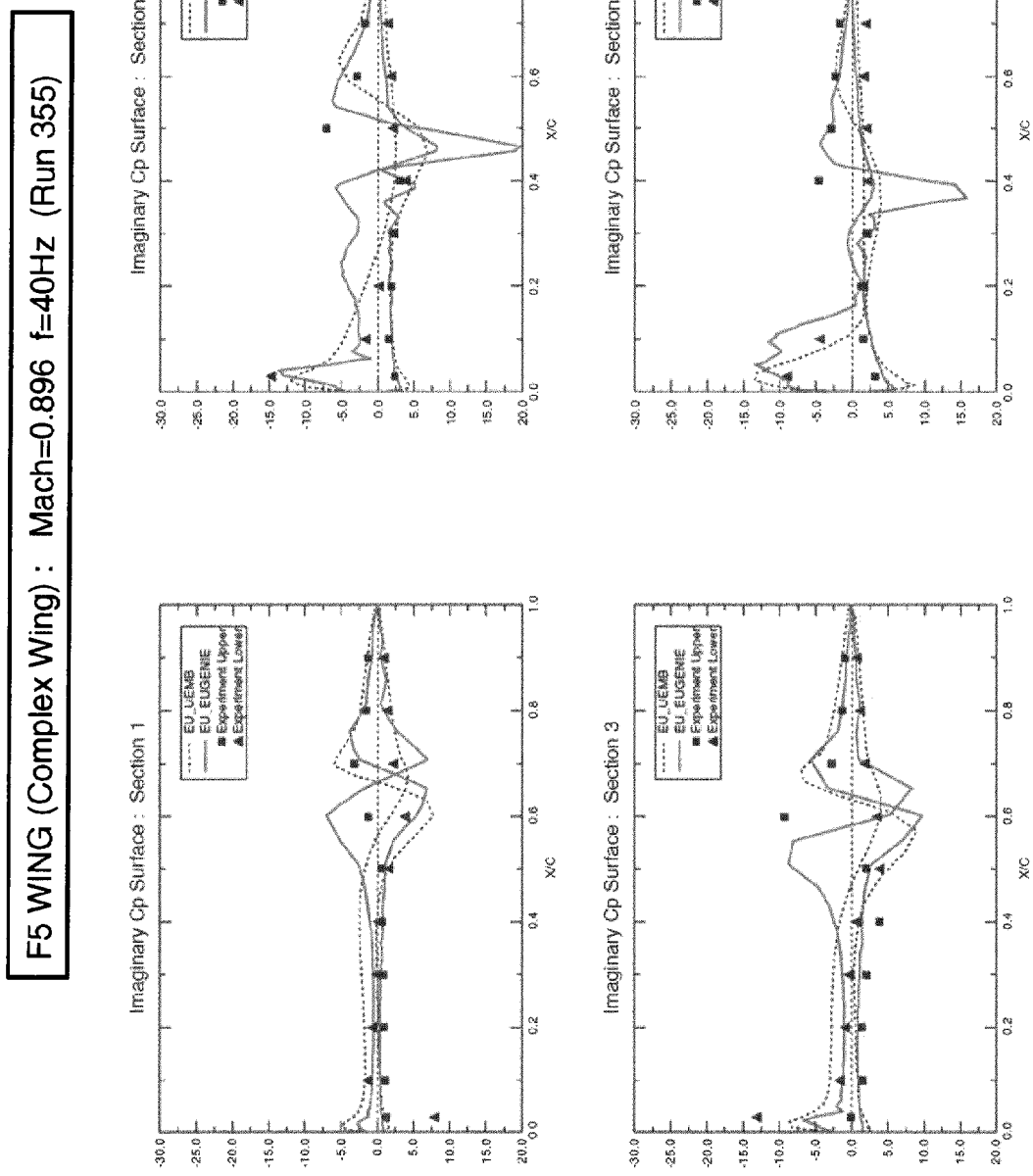

Figure 19 **Code Comparison, unsteady flow. Run 355 (complex geometry, M=0.869, F=40 Hz, α=0.004°,θ=0.117°) CpImag vs. X/C for Euler methods (EUGENIE and UEMB) at sections 1, 3, 7 and 8.**

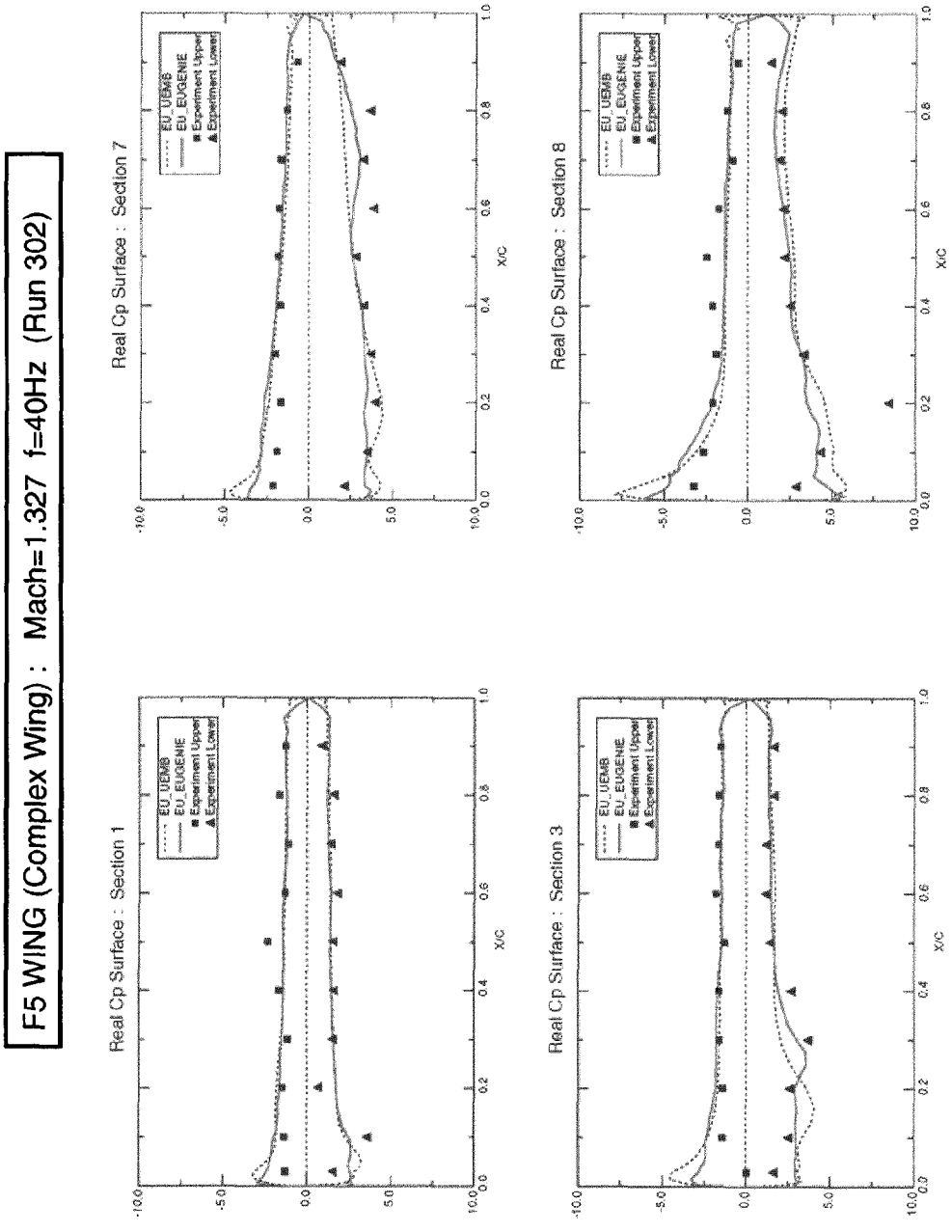

Figure 20 **Code Comparison, unsteady flow. Run 302 (complex geometry, M=1.327, F=40 Hz, α=0.16°, θ=0.221°) CpReal vs. X/C for Euler (EUGENIE and UEMB) at sections 1, 3, 7 and 8.**

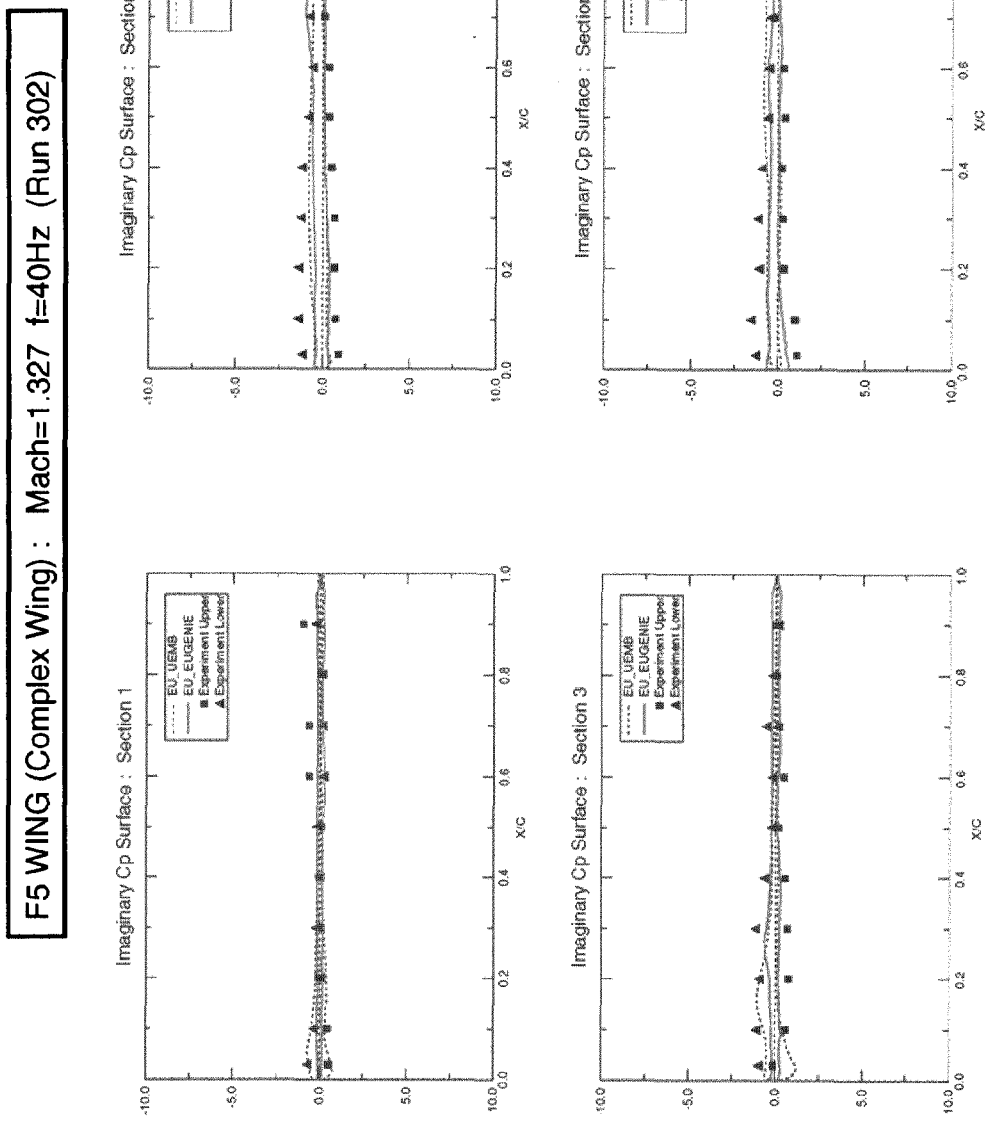

Figure 21 **Code Comparison, unsteady flow. Run 302 (complex geometry, M=1.327, F=40 Hz, α=0.16°, θ=0.221°) CpImag vs. X/C for Euler (EUGENIE and UEMB) at sections 1, 3, 7 and 8.**

REFERENCES

Ref. 1 Van Nunen J. W. G., Tijdeman H., et. al. (1978). 'Results of transonic wind tunnel measurements on an oscillating wing with external store (data report)', NLR TR 78030 U.

Ref. 2 Tijdeman H., Van Nunen J. W. G., et. al., (1978). 'Transonic wind tunnel tests of an oscillating wing with external store', Parts I-IV, NLR TR 78106 U.

Ref. 3 Pagano A., Renzoni P., Miller J. V., Hounjet M. H. L., Costes M., Le Balleur J. C., Gasparini L., Vigevano L., Kokkalis A., 'Formulation and Solution Algorithm of the Full Potential Code', HELISHAPE Report HELI/R/2/ONERA/02/A, June 1994.

Ref. 4 Costes M. & Le Balleur J. C., Gasparini L. & Vigevano L., Hounjet M. H. L., Kokkalis A. Miller J. V. & Spruce M., Pagano A. & Renzoni P., Rocchetto A., Toulmay F., 'Development of a Common European Unsteady Full Potential Code for Helicopter Rotors in Hover and Forward Flight', presented at American Helicopter Society 53rd Annual Forum, Virginia Beach, Virginia, April 29-May 1, 1997.

Ref. 5 Ruiz-Calavera L. P., 'Parametric Studies of a Time-Accurate Finite-Volume Euler code in the NWT parallel Computer'; AGARD-CP-578; Paper 38, 1995

Ref. 6 Batina, J. T.; Seidel, D. A.; Bland, S. R.; and Bennett, R. M., 'Unsteady Transonic Flow Calculations for Realistic Aircraft Configurations.' J. of Aircraft, vol. 26, no. 1, pp. 21-28, Jan. 1989.

Ref. 7 Schuster, D. M.; Vadyak, J.; and Atta, E.: *Static Aeroelastic Analysis of Fighter Aircraft Using a Three-Dimensional Navier-Stokes Algorithm.* Journal of Aircraft, vol. 27, no. 9, Sep. 1990, pp. 820-825.

Ref. 8 Schuster, D.M., Vadyak, J., and Atta, E., *Flight Loads Prediction Methods for Fighter Aircraft.* WRDC-TR-89-3104, Wright Research and Development Center, Wright-Patterson Air Force Base, OH, November, 1989

Ref. 9 Schuster, D. M.; Beran, P. S.; and Huttsell, L. J.: *Application of the ENSDAE/Navier-Stokes Aeroelastic Method.* Paper No. 3 in Numerical Unsteady Aerodynamics and Aeroelastic Simulation, AGARD Report 822, Mar. 1998.

Ref. 10 Knott M. J., 'Transonic Aeroelastic Calculations in Both the Time and Frequency Domains', in AGARD-CP-507 (73rd SMP), Oct. 1991.

Ref. 11 Anderson W. K. and Batina J. T., 'Accurate solutions, parameter studies, and comparisons for the Euler and potential flow equations', paper no. 15 presented at the AGARD 62nd Meeting of the Fluid Dynamics Panel Symposium on Validation of Computational Fluid Dynamics, Lisbon, Portugal, May 2-5, 1988.

Ref. 12 Dubac L., Cantariti F., Woodgate M., Gribben B., Badcock K. J. and Richards B. E., 'Solution of the unsteady Euler equations using an implicit dual time method', AIAA Journal, Vol. 36, 1417, 1998.

Ref. 13 Jameson A., Schmidt W., and Turkel E., 'Numerical solutions of the Euler equations by finite volumne methods using Runge-Kutta time-stepping schemes', AIAA paper 81-1259, 1981.

ACKNOWLEDGEMENTS

Contributions to this exercise were received from working group members and others outside the working group; the following contributors are acknowledged: R. M. Bennett and D M Schuster (NASA), L. P. Ruiz-Calavera (INTA), A. Pagano (CIRA), M. Woodgate, K. Badcock and F Cantarti (University of Glasgow), D.D. McKiernan (BAe.), E Geurts (NLR).